Modelling of aviation kerosene droplet heating and evaporation using complete fuel composition and surrogates

Abgail P. Pinheiro[a,*], Oyuna Rybdylova[b], Ivan A. Zubrilin[c], Sergei S. Sazhin[b], Fernando Luiz Sacomano Filho[d], João Marcelo Vedovotto[a]

[a] *Fluid Mechanics Laboratory, School of Mechanical Engineering, Universidade Federal de Uberlândia, Av. João Naves de Ávila, 2121, Uberlândia, Minas Gerais 38400-902, Brazil*
[b] *Advanced Engineering Centre, School of Computing, Engineering and Mathematics, University of Brighton, Brighton BN2 4GJ, UK*
[c] *Samara National Research University, 34, Moskovskoye Shosse, Samara 443086, Russia*
[d] *Department of Mechanical Engineering, Escola Politécnica da Universidade de São Paulo, Av. Prof. Mello Moraes, 2231, São Paulo, SP 05508-030, Brazil*

Abstract

A Discrete Component Model (DCM), based on the analytical solutions to heat transfer and species diffusion equations, together with the Abramzon-Sirignano model are applied to analyse the droplet heating and evaporation of Jet A kerosene and its surrogates. The models are implemented into MFSim code, which opens the way for modelling of the droplet heating and evaporation process alongside other spray processes. The composition of Jet A fuel used in the analysis, with 61 components split into 7 hydrocarbon groups, is described. This composition is approximated by twelve previously developed surrogates. The number of components in these surrogates varies between two and nine, which is expected to lead to a significant reduction in CPU requirements for calculation of droplet heating and evaporation, when compared to surrogates typically used to describe Jet A droplets. The prediction ability of the MFSim code, with new models implemented into it, is validated against available experimental results. The surrogates best able to predict droplet evaporation time and temperature of the Jet A fuel with 61 components are identified. It is shown that the number of

*Corresponding author
Email address: abgail.pinheiro@gmail.com (Abgail P. Pinheiro)

terms in the series of analytical solutions for temperature and species mass fractions can be considerably reduced without affecting the accuracy of calculations.

Keywords: Droplet heating, Multicomponent evaporation, Numerical simulation, Aviation kerosene, Jet A, Surrogates

---

Nomenclature

b_n	parameter defined in Eq. (5)
c	specific heat capacity (J/(kg K))
D	binary diffusivity coefficient (m^2/s)
D_d	droplet diameter (m)
h	convection heat transfer coefficient (W/(m^2 K))
h_{Y_0}	parameter defined in Eq. (10)
I_n	integral defined in Eq. (5)
j	parameter defined in Eq. (7)
k	thermal conductivity (W/(m K))
K	evaporation constant (mm^2/s)
L	latent heat of evaporation (J/kg)
M	molar mass (kg/kmol)
$\dot{m}$	evaporation rate (kg/s)
n_T	number of eigenvalues used to calculate the series in Eq. 3
n_Y	number of eigenvalues used to calculate the series in Eq. 8
n_{layers}	number of layers
p	pressure (Pa)
q_{Y_n}	integral defined in Eq. (12)
Q_{Y_n}	parameter defined in Eq. (11)
r	normalised radial coordinate
R	distance from the droplet centre (m)
R_d	droplet radius (m)

t	time (s)
T	temperature (K)
V	molar volume (m^3/kmol)
Y	mass fraction

Greek symbols

α_m	parameter defined in Eq. (10) (m/s)
α_{BSM}	accuracy of the bisection method
χ	molar fraction
Δt	time step (s)
ϵ_i	species evaporation rate
κ	parameter defined in Eq. (6) (1/s)
λ_n	eigenvalues obtained from the solution to Eqs. (4) and (9)
μ	dynamic viscosity (kg/(m s))
ν_{Y_n}	eigenfunctions defined in Eq. (13)
ϕ	relative deviation
ρ	density (kg/m^3)
σ	Lennard-Jones length ($\mathring{A}$)
ζ	parameter defined in Eq. (6) (K)

Subscripts

av	average
c	centre
cr	critical
d	droplet
eff	effective
evap	evaporation
exec	execution
g	gas
i	species

l	liquid
m	gas-vapour mixture
max	maximum
s	surface
sat	saturated
v	vapour
0	value at the beginning of a time step

1. Introduction

Droplet heating and evaporation are known to play a crucial role in liquid-fueled internal combustion devices [1]. The most widely used fuels worldwide, including gasoline, diesel fuel and kerosene, are petroleum products containing many hydrocarbon components. Different components evaporate at different rates, creating concentration gradients in the liquid phase and, therefore, causing species diffusion inside the droplets [2, 3]. The more volatile substances at the droplet surface evaporate first, leaving the less volatile components that evaporate slowly. Thus, composition and distribution of liquid species inside droplets can vary significantly during their lifetime. Typical relaxation times of species concentrations inside droplets are generally much longer than temperature relaxation times and they are comparable with the droplet lifetimes [3, 4]. Therefore, species diffusion processes need to be taken into account when modelling multicomponent droplet heating and evaporation [5].

This paper focuses on the modelling of aviation kerosene droplets, more specifically Jet A, which is currently one of the most widely used types of civilian gas turbine aviation kerosene [6]. This liquid fuel includes many dozens of components, so for realistic engineering sprays, rigorous modelling of the contribution of each component might be problematic, due to the excessive CPU requirements. To address this issue, various simplifications have been proposed in the literature aiming to reduce the number of variables and, thus, the

computational expense. The Distillation Curve Model [7] and the Continuous Thermodynamics Model [8], have been widely used, but their major limitation is that both models are based on the assumption of infinitely fast diffusivity of species inside droplets [3]. The Multi-Dimensional Quasi-Discrete Model suggested in [5], and further developed in [9], takes into account the diffusion of species inside droplets and it could be potentially applied for modelling Jet A droplet heating and evaporation without excessive CPU requirements [9]. This model, however, is based on the introduction of quasi-components with non-integer values of carbon numbers, which limits its application to the modelling of ignition and general combustion processes.

A promising approach to the approximation of Jet A, which would allow the modelling of heating and evaporation of droplets, as well as ignition and combustion of fuel vapour-air mixture, could be to replace this fuel with a surrogate. Results of preliminary research in this direction are presented in [10]. The authors of this paper considered a number of kerosene surrogates, selected mainly based upon their ignition and combustion characteristics, and they investigated how well heating and evaporation of kerosene droplets can be predicted if using the surrogates as opposed to the composition presented in [11]. The fact that the authors of [10] did not make a distinction between the different types of kerosene limits the applicability of their analysis. Additionally, some simplifications used in the analysis presented in [10] turned out to be too crude for accurate investigation of droplet heating and evaporation.

The present research addresses essentially the same problem as considered in [10], but using a rather different approach to its solution. Firstly, the analysis is restricted to Jet A and surrogates developed specifically for this fuel. Secondly, a number of improvements to the model used in [10] have been made, which are described later in the paper. Thirdly, the model was implemented in the in-house code MFSim [12, 13, 14, 15], which is written in the C programming language, opening the way for modelling the droplet heating and evaporation process alongside other spray processes.

The paper is organized as follows. In Sections 2 and 3, the mathematical

model for multicomponent droplet heating and evaporation is presented with numerical and computational details. The composition of Jet A and its surrogates are described in Section 4. In Section 5, transport and thermodynamic properties of both liquid and vapour phases are summarised. In Section 6, the results of calculations are presented and discussed. Section 7 summarises the main new results presented in the paper.

2. Mathematical model

The Abramzon-Sirignano model [16], generalised to multicomponent droples in [17], is used for the analysis of the processes in the gas phase. Raoult's law for the mixture of hydrocarbons is assumed to be valid:

$$p_{v,i_s} = \chi_{l,i_s} p^*{}_{v,i}, \tag{1}$$

where χ_{l,i_s} is the molar fraction of the ith component in the liquid phase at the droplet surface, p_{v,i_s} and $p^*{}_{v,i}$ are the partial vapour pressure of the ith component at the droplet's surface and the partial pressure of the same component in the absence of other components ($\chi_{l,i_s} = 1$), respectively. Transport and thermodynamic properties in the gas phase are estimated in the film region where temperature and mass fractions of the components are estimated based on the 1/3 averaging rule [18, 19].

The effect of the temperature gradient in a droplet's interior is taken into account by means of the analytical solution to the one-dimensional heat conduction equation with the Robin boundary condition at the droplet surface:

$$h(T_{\text{eff}} - T_s) = k_l \left.\frac{\partial T}{\partial R}\right|_{R=R_d-0}, \tag{2}$$

which is presented as [3, 20]:

$$T(r,t) = \frac{1}{r}\sum_{n=1}^{\infty}\left\{\left(I_n - \frac{\sin\lambda_n}{\lambda_n^2}\zeta\right)\frac{\exp\left(-\kappa\lambda_n^2 t\right)}{b_n}\right\}\sin\left(\lambda_n r\right) + T_{\text{eff}}, \tag{3}$$

where $r = R/R_d$ is the normalised radial coordinate from the droplet centre, λ_n are positive roots of the following equation arranged in ascending order:

$$\lambda \cos \lambda + j \sin \lambda = 0, \tag{4}$$

$$b_n = \frac{1}{2}\left(1 + \frac{j}{j^2 + \lambda_n^2}\right), \; I_n = \int_0^1 r T_0\left(r\right) \sin\left(\lambda_n r\right) dr, \tag{5}$$

$T_0\left(r\right)$ is the initial temperature distribution inside the droplet or the distribution predicted at the previous time step:

$$\kappa = \frac{k_l}{c_{p,l}\rho_l R_d^2}, \;\; \zeta = \frac{h T_{\text{eff}} R_d}{k_l}, \tag{6}$$

$$T_{\text{eff}} = T_g + \frac{\dot{m}_d L}{4\pi R_d^2 h}, \;\; j = \frac{h R_d}{k_l} - 1, \tag{7}$$

and h is the convection heat transfer coefficient.

Solution (3) was incorporated into the numerical code and it is updated at each time step in the calculations. The results achieved with Eq. (3) were shown to be the same as the results achieved based on the numerical solution of the corresponding one-dimensional heat conduction equation inside a spherical droplet [3].

The effect of the species mass fraction gradient within a droplet is taken into account based on the analytical solution to the one-dimensional species diffusion equation with the corresponding boundary condition at the droplet surface [3]:

$$Y_{l,i}\left(r,t\right) = \varepsilon_i + \frac{1}{r}\left\{\exp\left[D_l\left(\frac{\lambda_0}{R_d}\right)^2 t\right]\left[q_{Y_0,i} - Q_{Y_0}\varepsilon_i\right]\sinh\left(\lambda_0 r\right) + \right.$$
$$\left. + \sum_{n=1}^{\infty}\left[\exp\left[-D_l\left(\frac{\lambda_n}{R_d}\right)^2 t\right]\left[q_{Y_n,i} - Q_{Y_n}\varepsilon_i\right]\sin\left(\lambda_n r\right)\right]\right\}, \tag{8}$$

where λ_0 and λ_n for $n \geq 1$ are solutions to the equations:

$$\tanh\lambda = -\frac{\lambda}{h_{Y_0}} \quad \text{and} \quad \tan\lambda = -\frac{\lambda}{h_{Y_0}}, \tag{9}$$

respectively,

$$h_{Y_0} = -\left(1 + \frac{\alpha_m R_d}{D_l}\right), \;\; \alpha_m = \frac{|\dot{m}_d|}{4\pi\rho_l {R_d}^2}, \tag{10}$$

$$Q_{Y_n} = \begin{cases} -\frac{1}{\|\nu_{Y_0}\|^2} \frac{\left(1+h_{Y_0}\right)\sinh\lambda_0}{{\lambda_0}^2}, & \text{when} \quad n=0, \\ \frac{1}{\|\nu_{Y_n}\|^2} \frac{\left(1+h_{Y_0}\right)\sin\lambda_n}{{\lambda_n}^2}, & \text{when} \quad n \geq 1, \end{cases} \tag{11}$$

$$q_{Y_n,i} = \frac{1}{\|\nu_{Y_n}\|^2} \int_0^1 r Y_{l,i_0}(r)\, \nu_{Y_n} dr, \quad \text{for} \quad n \geq 0, \tag{12}$$

$Y_{l,i_0}(r)$ are the initial species mass fraction distributions inside the droplet or the distributions predicted at the previous time step,

$$\nu_{Y_n} = \begin{cases} \sinh(\lambda_0 r), & \text{when} \quad n=0, \\ \sin(\lambda_n r), & \text{when} \quad n \geq 1, \end{cases} \tag{13}$$

$$\|\nu_{Y_n}\|^2 = \begin{cases} -\frac{1}{2}\left[1 + \frac{h_{Y_0}}{{h_{Y_0}}^2 - {\lambda_0}^2}\right], & \text{when} \quad n=0, \\ \frac{1}{2}\left[1 + \frac{h_{Y_0}}{{h_{Y_0}}^2 + {\lambda_n}^2}\right], & \text{when} \quad n \geq 1. \end{cases} \tag{14}$$

As in the case of Solution (3), Solution (8) was incorporated into the numerical code and was used at each time step in the calculations. The results achieved with Eq. (8) were shown to be the same as the results achieved based on the numerical solution of the corresponding one-dimensional species diffusion equation inside a spherical droplet [3].

Both analytical solutions for temperature and species mass fraction were obtained assuming that droplet radius is constant, which is justified for sufficiently short time steps, assuming that the surface regression rate is much smaller than the transport rate in the liquid [21]. At this stage, the model is applied to isolated stationary droplets. Its generalisation to moving droplets, using the Effective Thermal Conductivity/Effective Diffusivity (ETC/ED) model would be straightforward [3]. Also, the interaction between droplets could be taken into account in some limiting cases [3].

3. Implementation of the model into MFSim code

The model described in the previous section was implemented into in-house code MFSim, written in the C programming language. All calculations were

performed using an Intel(R) Core(TM) i7-3612QM CPU @ 2.10 GHz processor with a 100 MHz clock.

The main steps of the numerical algorithm are summarised by:

1. Initially, distributions of temperature and mass fractions of species inside the droplet are assumed uniform, and the initial molar fractions of species presented in Table 1 are adopted. For the subsequent time steps, the distributions obtained in the previous time step are used.
2. Calculation of the species partial pressures at the droplet surface using the supplementary data and Eq. (1).
3. Calculation of the species evaporation rates using the supplementary data and Eq. (19).
4. Determination of the reference conditions of the gas-vapour mixture.
5. Calculation of the mixture properties μ_m, ρ_m, $D_{v,m}$, k_m and c_{p_m} using the Cantera database.
6. Calculation of the gas properties ρ_g, μ_g and k_g using the Cantera database.
7. Calculation of the fuel vapour property c_{p_v} using the Cantera database.
8. Calculation of the liquid properties ρ_l, c_l, k_l, μ_l and D_l using the expressions in the supplementary data and the equations presented in Section 5.
9. Calculation of the dimensionless numbers, the total evaporation rate and the contribution of each component.
10. Calculation of the effective temperature, κ and ζ using Eqs. (7) and (6).
11. Calculation of the distribution of temperature inside the droplet based on Eq. (3). The roots of Eq. (4) are found using the bisection method [22].
12. Calculation of the droplet average temperature using Simpson's method [22].
13. Calculation of the distribution of species inside the droplet based on Eq. (8). The roots of Eq. (9) are found using the bisection method [22].
14. Calculation of the droplet average composition using Simpson's method [22].

15. Update ρ_l based on the change in droplet average temperature and average composition.

16. Update the droplet diameter using the 4th-order Runge-Kutta scheme [22] and taking into account both its evaporation and thermal swelling.

17. Return to Step 1 and repeat all steps for the next time step.

Table 1: Molar fractions of the components of Jet A. C_n stands for carbon number, n-par for n-paraffins, iso-par for iso-paraffins, monocyclo for monocycloparaffins, dicyclo for dicycloparaffins, alkyb for alkylbenzenes, cycloa for cycloaromatics, alkylnaph for alkylnaphthalenes.

C_n	n-par	iso-par	monocyclo	dicyclo	alkyb	cycloa	alkylnaph
C_7	0	0	0.0034	0	0	0	0
C_8	0.0109	0.0037	0.0500	0.0031	0.0010	0	0
C_9	0.0590	0.0581	0.0531	0.0094	0.0223	0.0018	0
C_{10}	0.0523	0.0731	0.0438	0.0110	0.0543	0.0088	0.0013
C_{11}	0.0322	0.0514	0.0277	0.0105	0.0331	0.0177	0.0043
C_{12}	0.0209	0.0325	0.0200	0.0072	0.0199	0.0210	0.0061
C_{13}	0.0154	0.0285	0.0137	0.0022	0.0146	0.0108	0.0038
C_{14}	0.0096	0.0199	0.0053	0.0011	0.0082	0.0058	0.0007
C_{15}	0.0054	0.0139	0.0009	0	0.0026	0.0001	0.0001
C_{16}	0.0024	0.0062	0	0	0.0013	0	0
C_{17}	0.0006	0.0014	0	0	0.0001	0	0
C_{18}	0.0001	0.0004	0	0	0	0	0

4. Compositions of Jet A and surrogates

The composition of Jet A, taken from Vozka *et al.* [23], is presented in Fig. 1 and Table 1. The analysis performed by the authors of [23] was based on 'two-dimensional gas chromatography a with flame ionization detector'. Altogether, 61 components were identified, which were split into 7 hydrocarbon groups.

The detailed description of the 61 components is hereafter referred to as the 'complete composition'.

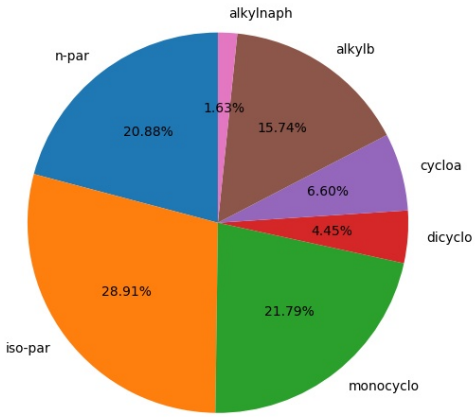

Figure 1: A schematic presentation of the composition of Jet A in terms of the molar fractions presented in Table 1.

To the best of the authors' knowledge, the first attempt to investigate heating and evaporation characteristics of kerosene surrogate droplets, using the model described in Section 2, was undertaken in [10]. The authors of that paper compared thirteen surrogates without making a distinction between standard kerosene and Jet A surrogates. For the present analysis, twelve Jet A surrogates developed over the last decade, between 2010 and 2019, were selected, without any overlap with surrogates considered in [10]. This aspect makes the present research a complementary study to the one conducted in [10].

The twelve previously developed surrogates used in the present analysis are listed in Table 2. As can be seen from this table, the number of components in these surrogates varies between two and nine, which is expected to lead to a significant reduction in CPU requirements for the calculation of droplet heating and evaporation compared with that for Jet A droplets containing 61 components [23].

In all cases, the selection of surrogates was based mainly on the similarity

Table 2: Jet A surrogates selected for the present analysis, their brief description, the numbers of components in them, and the references to the papers in which they were first described.

Surrogates	Description	N Comp	References
1	Dooley's 1st generation	3	[24]
2	Huber's surrogate	8	[25]
3	Dooley's 2nd generation	4	[26]
4	Kim's UM1	4	[27]
5	Kim's UM2	4	[27]
6	Improved Dooley's 1st gen.	3	[28]
7	Improved Dooley's 2nd gen.	4	[28]
8	Won's 1st surrogate	3	[29]
9	Won's 2nd surrogate	3	[29]
10	Won's 3rd surrogate	4	[29]
11	Won's 4th surrogate	9	[29]
12	Jameel's surrogate	2	[30]

between the key properties of the surrogates and Jet A. There was specific justification, however, for the selection of each surrogate. The components of Surrogate 1, called Dooley's 1st generation surrogate, were selected based on several combustion related properties, including cetane number, ratio of the numbers of hydrogen and carbon atoms, sooting propensity and average molecular weight. The selection of the components of Surrogate 2, on the other hand, focused on thermophysical properties, such as density, viscosity, thermal conductivity, and volatility. Surrogate 3 is known as Dooley's 2nd generation surrogate. Even though its formulation is based on the same target properties of Surrogate 2, it prioritises emulation of the average molecular weight, as both physical properties and combustion kinetic phenomena are highly influenced by the molecular structure.

The selection of components of Surrogates 4 and 5 was based on the same

target criteria, including cetane number, net calorific value, hydrogen to carbon ratio, average molecular weight, density, viscosity, surface tension, and distillation curve, but with different weights for each criterion. Surrogate 4 reproduces better temperature-independent properties, i.e. the first four target criteria from the ones listed above, while Surrogate 5 was shown to better emulate liquid density and volatility. Surrogates 6 and 7 are generally referred to as improved versions of Surrogates 1 and 3, respectively, the Dooley's surrogates, as they were developed based on a new surrogate formulation method. The novelty of this method lies in constructing surrogates by directly matching molecular structures and key functional groups instead of using combustion parameters explicitly.

The selection of Surrogates 8 to 11 was based on statistical analysis of the relation between each chemical functional group and a specific combustion property of the fuel. Although the combustion behaviour of the four surrogates is similar, their physical properties show considerable variation. This is particularly visible in the case of the distillation characteristics, which dictate preferential evaporation effects. Finally, Surrogate 12 was designed using a 'minimalist functional group approach', which focuses on matching fundamental molecular parameters rather than broad molecular classes. Also, this new surrogate formulation method limited the number of components to two.

The chemical formulae of the components used in surrogates, their names and Chemical Abstracts Service (CAS) numbers are presented in Table 3. Note that the CAS number for 1-methyldecalin is not available. Molar fractions of the components in the surrogates are presented in Table 4. Data provided in Table 4 are used for the analysis of surrogate droplet heating and evaporation.

As follows from this brief overview, in all cases the surrogates were selected based on specific properties of interest. A comprehensive investigation of the other properties of each selected surrogate and the comparison of these properties with those of Jet A have still to be undertaken.

Table 3: The components used in the Jet A surrogates, their chemical formulae, names and Chemical Abstracts Service (CAS) numbers.

Comps	Formulae	Names	CAS numbers
1	C_8H_{18}	n-octane	111-65-9
2	$C_{10}H_{22}$	n-decane	124-18-5
3	$C_{12}H_{26}$	n-dodecane	112-40-3
4	$C_{14}H_{30}$	n-tetradecane	629-59-4
5	$C_{16}H_{34}$	n-hexadecane	544-76-3
6	C_7H_{16}	iso-heptane	591-76-4
7	C_8H_{18}	iso-octane	592-27-8
8	$C_{12}H_{26}$	iso-dodecane	7045-71-8
9	$C_{16}H_{34}$	iso-cetane	1560-93-6
10	C_7H_{14}	methylcyclohexane	108-87-2
11	$C_{13}H_{26}$	heptylcyclohexane	5617-41-4
12	$C_{10}H_{18}$	decalin	493-02-7
13	$C_{11}H_{20}$	1-methyldecalin	-
14	$C_{11}H_{20}$	2-methyldecalin	4683-94-7
15	$C_{11}H_{20}$	5-methyldecalin	2547-27-5
16	C_7H_8	toluene	108-88-3
17	C_8H_{10}	o-xylene	95-47-6
18	C_9H_{12}	propylbenzene	103-65-1
19	C_9H_{12}	1,3,5-trimethylbenzene	108-67-8
20	$C_{13}H_{20}$	heptylbenzene	1078-71-3
21	$C_{10}H_{12}$	tetralin	119-64-2

5. Thermodynamic and transport properties of the components

The transport and thermodynamic properties of fuel vapour and ambient gas, including density, dynamic viscosity, thermal conductivity, specific heat capacity, and binary diffusion coefficient, are obtained from the open source

Table 4: Molar fractions of the components used in each Jet A surrogate (in per cent).

	Surrogates											
Comps	1	2	3	4	5	6	7	8	9	10	11	12
1	-	-	-	-	-	-	-	-	-	-	2.30	-
2	42.67	-	-	-	-	54.71	-	-	-	-	5.00	-
3	-	-	40.40	38.44	28.97	-	48.57	49.00	-	31.20	29.90	-
4	-	5.70	-	-	-	-	-	-	-	-	10.00	-
5	-	3.30	-	-	-	-	-	-	36.50	12.30	1.40	-
6	-	-	-	-	-	-	-	-	-	-	-	69.10
7	33.02	-	29.50	-	-	20.75	22.86	21.00	31.00	-	3.40	-
8	-	-	-	-	-	-	-	-	-	24.30	14.30	-
9	-	-	-	14.84	14.24	-	-	-	-	-	-	-
10	-	-	-	23.36	-	-	-	-	-	-	-	-
11	-	27.9	-	-	-	-	-	-	-	-	-	-
12	-	-	-	-	31.88	-	-	-	-	-	-	-
13	-	1.30	-	-	-	-	-	-	-	-	-	-
14	-	15.40	-	-	-	-	-	-	-	-	-	-
15	-	16.50	-	-	-	-	-	-	-	-	-	-
16	24.31	-	-	23.36	24.91	24.54	-	-	-	-	5.20	-
17	-	7.10	-	-	-	-	-	-	-	-	-	-
18	-	-	22.80	-	-	-	23.81	-	-	-	-	-
19	-	-	7.30	-	-	-	4.76	30.00	32.50	32.20	28.50	-
20	-	-	-	-	-	-	-	-	-	-	-	30.90
21	-	22.80	-	-	-	-	-	-	-	-	-	-

Cantera software package [31, 32]. All properties are mixture averaged based on molar composition. The Cantera input file that provides information for each component is provided in the supplementary data.

The transport and thermodynamic properties of liquid hydrocarbons, including density, dynamic viscosity, thermal conductivity, and specific heat capacity, alongside latent heat of evaporation, saturated vapour pressure, critical temperature, and pressure, are inferred from the databases in Yaws' books [33, 34, 35]. These properties for the Jet A liquid components are calculated at the average temperature inside the droplets, while latent heat of evaporation and saturated

vapour pressure are calculated at the droplet surface temperature. The approximations inferred from [33, 34, 35] and used in the present analysis are presented in the supplementary data.

The Wilke-Chang approximation for the liquid species diffusion coefficient is used [36]:

$$D_{l,i} = \frac{7.4 \times 10^{-15} \sqrt{M_l} T}{\mu_l {V_{l,i}}^{0.6}}, \tag{15}$$

where M_l is average molar mass of the liquid mixture:

$$M_l = \left[\sum_i \left(\frac{Y_{l,i}}{M_{l,i}} \right) \right]^{-1}, \tag{16}$$

$$V_{l,i} = \left(\frac{\sigma_{l,i}}{1.18} \right)^3, \tag{17}$$

$\sigma_{l,i}$ is the Lennard-Jones length for the ith component, in $\mathring{A}$ [37]:

$$\sigma_{l,i} = 0.17791 + 11.779 \left(\frac{T_{\mathrm{cr},i}}{p_{\mathrm{cr},i}} \right) - 0.049029 \left(\frac{T_{\mathrm{cr},i}}{p_{\mathrm{cr},i}} \right)^2, \tag{18}$$

critical temperatures $T_{\mathrm{cr},i}$ and critical pressures $p_{\mathrm{cr},i}$ of the components are in K and bar, respectively.

The properties of the mixtures were estimated as [5]:

$$L = \sum_i \left(\varepsilon_i L_i \right), \quad {p_v}_s = \sum_i \left(\chi_{l,i} {p_{v,i}}_s \right), \tag{19}$$

$$\rho_l = \left[\sum_i \left(\frac{Y_{l,i}}{\rho_{l,i}} \right) \right]^{-1}, \quad \ln \mu_l = \sum_i \left(\chi_{l,i} \ln \mu_{l,i} \right), \tag{20}$$

$$k_l = \left[\sum_i \left(\frac{Y_{l,i}}{{k_{l,i}}^2} \right) \right]^{-1/2}, \quad c_l = \sum_i \left(Y_{l,i} c_{l,i} \right), \quad D_l = \sum_i \left(\chi_{l,i} D_{l,i} \right). \tag{21}$$

The thermodynamic and transport properties are assumed constant during each time step, but they vary from one time step to another due to the changes in temperature and composition.

6. Results and discussion

6.1. Modelling versus experimental data

To validate the predictions of the model described in Section 2 the experimental data for aviation kerosene (Jet A) provided in [38] is used. The main reason for selecting this paper is its focus on aviation kerosene; it shows that aviation kerosene droplets evaporate more slowly than common kerosene ones. In contrast, previous experimental studies have focused upon common kerosene droplet heating and evaporation (e.g. [39], [40], [41], [42]).

The experiment described in [38] was performed in a heated furnace in which the droplet was suspended from a nickel-chromium alloy wire of 200 μm diameter. The initial droplet temperature was the room temperature, assumed to be equal to 298 K, and the initial droplet diameter was 1.38 mm. The ambient pressure was atmospheric, assumed to be equal to 0.1 MPa, and the furnace temperature was monitored by a thermocouple and maintained at 573 K. Both the droplet and the ambient air were quiescent.

In the present study, the droplet volume was discretised into 500 concentric layers to calculate the integrals in Solutions (3) and (8), whereas time steps of 1×10^{-5} s were considered. 200 eigenvalues were used to calculate the temperature distribution and 100 eigenvalues were used to calculate the species mass fraction distributions. The roots of the equation for eigenvalues were found using the bisection method with accuracy of 1×10^{-12}. The results of sensitivity analysis based on the choice of these parameters are presented in the next section.

As follows from Table 1 of [20], when the number of layers used in calculations is less than 50, the predictions of the model are dependent upon that number, but they do not change when the number of layers is between 50 and 500. Since the conditions of the present simulations are not the same as in the setup analysed in [20], 500 layers are used in the present analysis to mitigate this effect. As can be seen in Figure 4 of [43], using 10 eigenvalues leads to unacceptably large errors when predicting the values of mass fractions of the components near the centre and the surface of the droplets, whilst using 40 eigenvalues led to

reasonably accurate predictions of these mass fractions within the whole volume of the droplet. This justifies the decision to use 50 eigenvalues in the present analysis. A discussion on computational cost and a further investigation of how the numerical parameters influence the results are presented in Section 6.3 (see Table 5).

Fig. 2 shows a comparison of the normalised squared droplet diameter *versus* time obtained from the numerical simulations and the experimental data, while Fig. 3 presents plots of temperature at the droplet surface and at its centre, as well as the average temperature predicted by the numerical simulations.

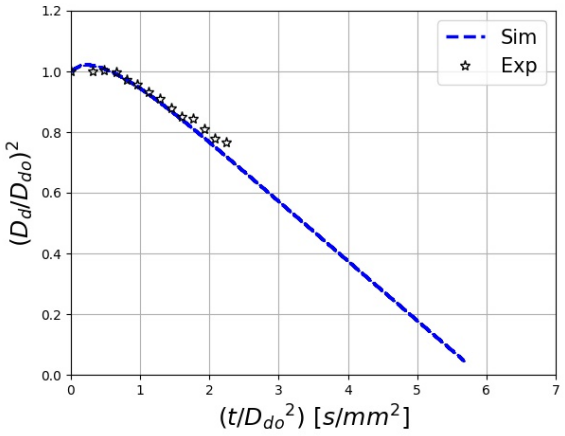

Figure 2: Normalised squared droplet diameter *versus* time predicted by the present simulation (dashes) and the results of measurements [38] (stars).

As follows from Fig. 2, the results of simulations agree reasonably well with experimental data, giving confidence in the present modelling approach. In agreement with experimental data, the simulations show initial thermal swelling, which is followed by a steady evaporation period. Although a Jet A droplet contains a mixture of many components, its evaporation characteristics can be well approximated by the D^2 law. Fig. 3 shows that, at the beginning of the droplet heating and evaporation process, the droplet surface temperature increases more quickly than the droplet average and centre temperatures. Then

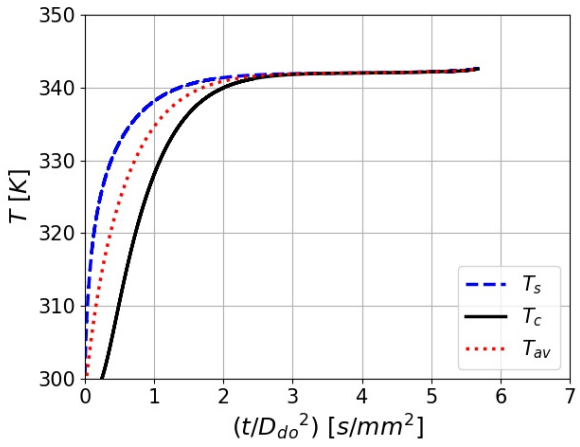

Figure 3: Droplet surface, centre and average temperatures *versus* time predicted by the present simulation.

follows a rather long 'plateau' period when the values of these temperatures coincide and there is almost no change over time. This 'plateau' corresponds to the D^2 law for droplet evaporation clearly seen in Fig. 2. At the very end of the droplet evaporation period, an oscillatory increase in all three temperatures was identified. The model predictions at this stage, however, are not expected to be reliable due to the very small size of the droplet. Therefore, this oscillatory behaviour, which is non-physical, is not presented in Fig. 3.

Fig. 4 shows a comparison between the normalised squared droplet diameter *versus* time predicted using several modelling approaches and the experimental data, while Fig. 5 shows the droplet average temperature *versus* time predicted by these modelling approaches. In both figures, the term 'New comp' refers to the simulation results when the Jet A composition presented in Table 1 is used. The kerosene composition analysed by Lissitsina *et al.* [11], previously used by Poulton *et al.* [10] and identified as 'Old comp', is also shown here in order to demonstrate the effect of using different kerosene compositions. Additionally, the assumption made by Poulton *et al.* [10], that the vapour diffusion coefficient can be approximated by cycloundecane, is tested to understand how it would

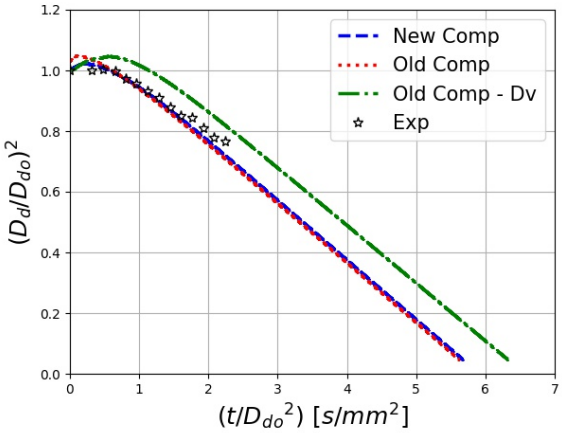

Figure 4: Normalised squared droplet diameter *versus* time predicted by the simulations (dashed curves) and the results of measurements [38] (stars). 'New comp' refers to Jet A composition from [23] presented in Table 1, 'Old comp' refers to kerosene composition from [11] (used in [10]) and 'Old comp - Dv' refers to the case when the cycloundecane approximation for the vapour diffusion coefficient was used.

affect the results. The results obtained taking this approximation into account are referred to in the plots as 'Old comp - Dv'.

As can be seen in Fig. 4, using the composition from [11] also delivers a good agreement with the experimental data. At the same time, one can see from this figure that the assumption that the vapour diffusion coefficient can be approximated by that of cycloundecane may not be the best choice, as in this case droplet diameter and temperature predictions clearly deviate from the experimental measurements. Note that Poulton *et al.* [10] used experimental measurements of common kerosene evaporation extracted from Javed *et al.* [41] to validate the simulations performed for the composition described by Lissitsina *et al.* [11] for aviation kerosene.

6.2. Analysis of surrogates

Droplet evaporation behaviours using the Jet A complete composition from Table 1 and surrogates from Table 4 are compared using the same boundary and initial conditions as in Section 6.1, $T_{d_0} = 298$ K, $D_{d_0} = 1.38$ mm, $p_g = 0.1$

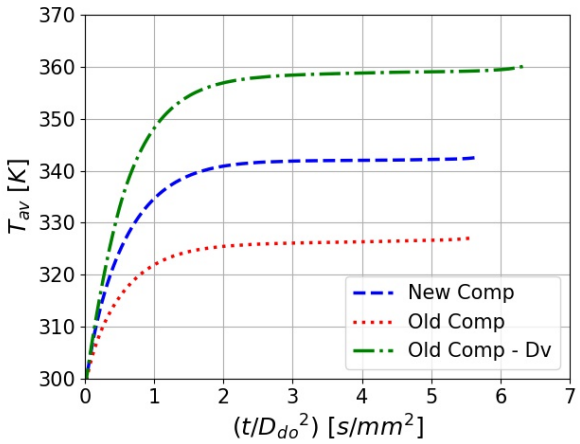

Figure 5: Droplet average temperature *versus* time for the same cases as presented in Figure 4. 'New comp' refers to Jet A composition from [23] presented in Table 1, 'Old comp' refers to kerosene composition from [11] (used in [10]) and 'Old comp - Dv' refers to the case when the cycloundecane approximation for the vapour diffusion coefficient was used.

MPa, and $T_g = 573$ K. These parameters are the same as the ones used in the experiment described in [38]. Figure 6 shows a comparison of the normalised squared droplet diameters and the droplet average temperature versus time inferred from the numerical simulations.

The results for the twelve surrogates are presented in three groups of plots. Surrogates 1, 6, 3 and 7 are grouped together since they are Dooley's 1st and 2nd generation surrogates; Surrogates 1 and 3 are the original ones and 6 and 7 are the improved ones. Surrogates 8, 9, 10 and 11 were all formulated by Won *et al.* [29] using the same statistical methodology based on chemical functional groups. The remaining Surrogates 2, 4, 5 and 12 are presented in the final pair of plots.

Plots of relative deviations between the evaporation times for the cases when the complete Jet A composition and surrogates were used (ϕ_t) are shown in Fig. 7. ϕ_t was estimated as:

$$\phi_t = \frac{t_{\text{evap,complete}} - t_{\text{evap,surrogate}}}{t_{\text{evap,complete}}} \times 100\%. \tag{22}$$

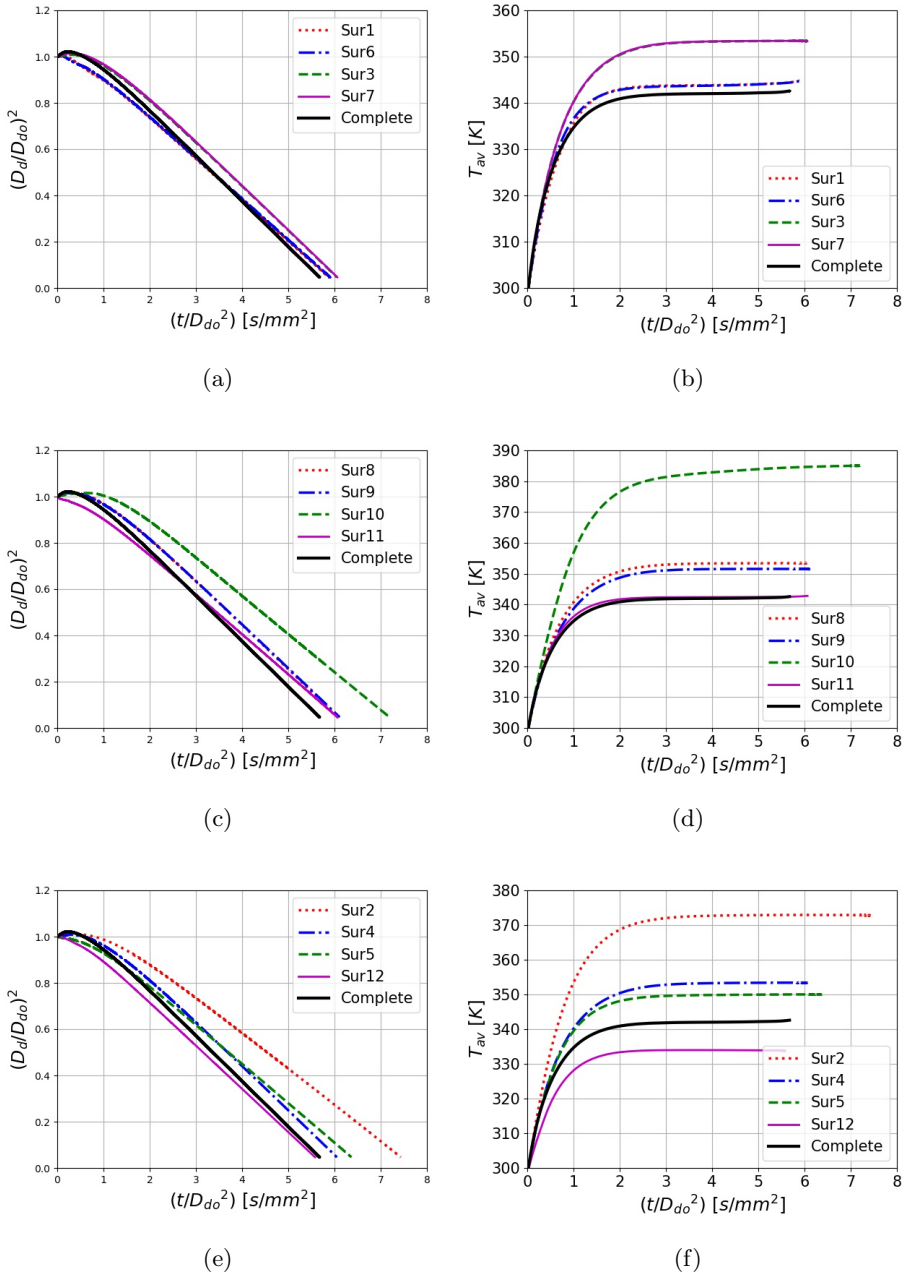

Figure 6: Normalised squared droplet diameter *versus* time (a, c, e) and droplet average temperature *versus* time (b, d, f) for droplets of complete composition and surrogates.

The values of $t_{\text{evap,complete}}$ and $t_{\text{evap,surrogate}}$ were estimated at the time instants when droplet volumes reached 10% of their initial values.

For Surrogates 1 to 11 evaporation times are longer than that calculated for the complete Jet A composition. For Surrogate 12, on the other hand, the evaporation time is 1.7% shorter than that calculated for the complete Jet A composition. For this surrogate, the absolute value of ϕ_t is the smallest. Even though Surrogate 2 focuses on thermophysical properties, the results of calculations for this surrogate show the biggest deviation for evaporation time, with a droplet lifetime 30.6% longer than that predicted for a droplet with the complete fuel composition. This happens because this surrogate was developed prioritising components with higher boiling points. The droplets of Surrogate 10 are predicted to take 26.5% longer to evaporate than those with the complete fuel composition. Although this surrogate is specifically intended to emulate the Jet A distillation curve, is also designed to replicate the Jet A molecular weight, and this adversely affects its performance. The models using Surrogates 2 and 10 tend to predict higher equilibrium temperatures, as seen in Fig. 6, due to the significant presence of species with higher boiling temperatures in their composition. Even though the droplet is heated to a higher temperature, the less volatile components take longer to completely evaporate.

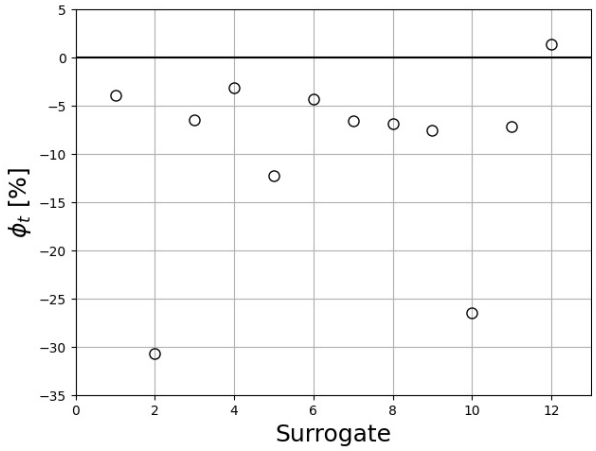

Figure 7: Relative evaporation time *versus* surrogate numbers.

When the well-known D^2 law is followed, as observed for Jet A droplet evaporation, the droplet surface area decreases linearly with time. The average area reduction rate, known as the evaporation constant K, can be estimated as a slope of the variation of the squared droplet diameter. Relative average area reduction rate for droplets of complete composition and surrogates was estimated as:

$$\phi_K = \frac{K_{\text{complete}} - K_{\text{surrogate}}}{K_{\text{complete}}} \times 100\%. \tag{23}$$

The results are shown in Fig. 8. The values of K_{complete} and $K_{\text{surrogate}}$ for each surrogate were calculated from the data presented in Fig. 6. The best-fit straight lines used to estimate K were found using least squares regression.

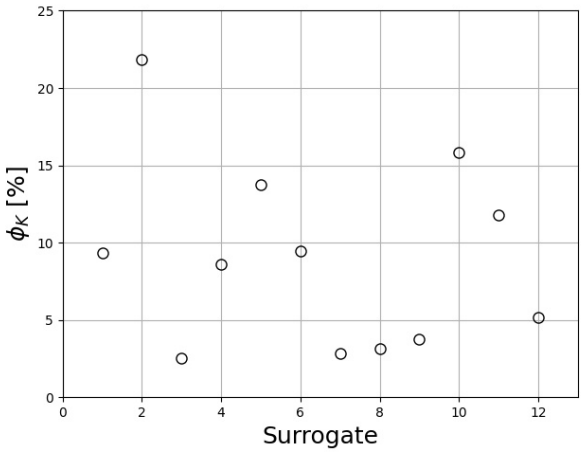

Figure 8: Relative average area reduction rate *versus* surrogate numbers.

For all surrogates the predicted droplet evaporation rates are lower than that of a droplet with complete fuel composition. For Surrogates 3 and 7, which are both Dooley's 2nd generation surrogates, these deviations are the smallest, at 2.5% and 2.7%, respectively. The highest deviations are observed for Surrogates 2 and 10, at 21.8% and 15.9%, respectively. These trends are similar to those which follow from the analysis of evaporation times.

Relative differences between the maximal values of average droplet temperatures calculated for complete fuel composition and surrogates are estimated as:

$$\phi_T = \frac{\phi T_{\text{complete}} - \phi T_{\text{surrogate}}}{\phi T_{\text{complete}}} \times 100\%, \tag{24}$$

$$\phi T = T_{\text{av,max}} - T_0, \tag{25}$$

where T_0 are the initial droplet temperatures, which were the same for all droplets, at 298 K. The plots of ϕ_T *versus* surrogate number are shown in Fig. 9. The values of maximum average temperatures $T_{\text{av,max}}$ for complete fuel composition and surrogates were obtained during the last time steps of the calculations.

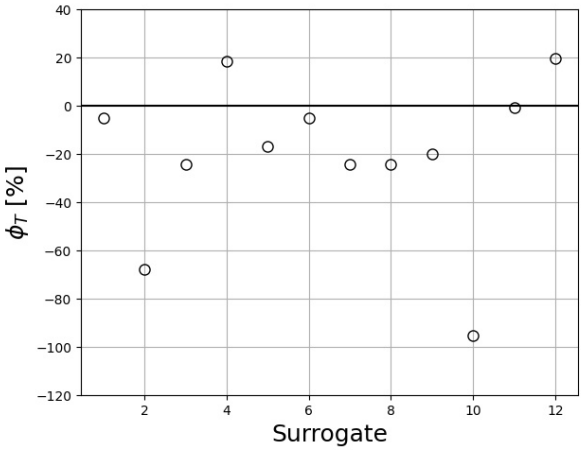

Figure 9: Relative temperature variation *versus* surrogate numbers.

As follows from Fig. 9, the highest absolute values of ϕ_T are predicted for Surrogates 2 and 10, which is consistent with the earlier results for droplet lifetimes and evaporation rates. The smallest absolute value of ϕ_T is predicted for Surrogate 11, at 0.5%.

In order to evaluate the computational cost of each numerical simulation, the execution time required to run 500 time steps was measured and the values acquired for each surrogate are shown in Fig. 10. This time turned out to be proportional to the number of components used in surrogates as shown in Fig. 11. The computational cost of simulations using Jet A complete composition, with

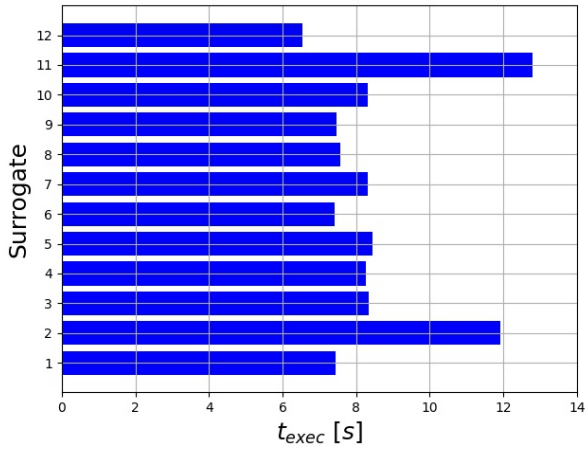

Figure 10: Execution time for each surrogate.

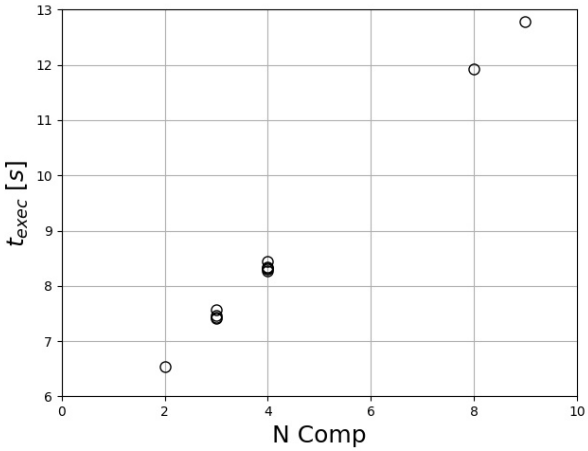

Figure 11: Execution time *versus* the number of components.

61 components, was always higher than that for surrogates. For example, to run 500 time steps using 61 components, it takes approximately 58.6 seconds, while in the case of 9 components, as in Surrogate 11, the required time is 4.6 times less. In the case of Surrogates 3 and 7, which have 4 components, the computational cost is about 7.1 times less. For Surrogate 12, with 2 components, the computational expense is 9 times less. This test considers only a single droplet.

For spray simulations tracking millions of droplets, using surrogates to achieve computational cost reduction would be a sensible choice.

6.3. Numerical analysis

Temperature and mass fraction distributions computed by the analytical solutions are affected by the number of terms used in the series, the numerical accuracy of calculating the eigenvalues and the number of layers used to calculate integrals in these series. In order to evaluate the influence of these parameters, and the time step (Δt) used in calculations, on the computational cost and on the accuracy of the results, 8 cases considering the complete Jet A composition were simulated, as presented in Table 5. The five parameters used in the present analysis are: the number of concentric layers used to discretise the droplet volume (n_{layers}), the absolute accuracy of the bisection method (α_{BSM}), the number of eigenvalues used to calculate the series in Eq. 3 (n_T), the number of eigenvalues used to calculate the series in Eq. 8 (n_Y) and the time step used in simulations.

The main focus of this section is to quantify how changing the above-mentioned five parameters affects the droplet diameter and temperature results, as well as the computational cost. All the simulations were conducted taking into consideration the same boundary and initial conditions as in Section 6.1, $T_{d_0} = 298$ K, $D_{d_0} = 1.38$ mm, $p_g = 0.1$ MPa, and $T_g = 573$ K. The time required for the droplet to reduce to 10% of its initial volume (t_{evap}) is considered, as well as the temperature difference at 5 s after the start of heating ($\phi T_{t=5s}$), namely the difference between the initial temperature and the average plateau temperature. Firstly, the values of both parameters, t_{evap} and $\phi T_{t=5s}$, are computed for Case 1, for which the finest mesh and the shortest time steps are used. For this case, $t_{\text{evap}} = 10.72$ s and the average temperature at 5 s was 341.2 K, which represented $\phi T_{t=5s} = 43.2$ K. The computational cost is evaluated as the execution time needed to run 10 ms of the droplet lifetime t_{exec} for each case. Since Δt varied, the number of time steps required to reach the target time of 10 ms also varied. The data for each case is presented in Table 5.

The accuracy of calculations was assessed based on the relative errors of calculation of $t_{\rm evap}$ and $\phi T_{t=5s}$ in relation to Case 1:

$$\tilde{t}_{\rm evap} = \frac{t_{\rm evap,Case1} - t_{\rm evap}}{t_{\rm evap,Case1}} \times 100\%, \tag{26}$$

$$\tilde{\phi T}_{t=5s} = \frac{\phi T_{t=5s,\rm Case1} - \phi T_{t=5s}}{\phi T_{t=5s,\rm Case1}} \times 100\%. \tag{27}$$

Table 5: Analysis of the effects of numerical parameters for 8 cases.

Case	$n_{\rm layers}$	$\alpha_{\rm BSM}$	n_T	n_Y	Δt [s]	$\tilde{t}_{\rm evap}$ [%]	$\tilde{\phi T}_{t=5s}$ [%]	$t_{\rm exec}$ [s]
1	1000	10^{-12}	200	100	1×10^{-6}	-	-	4133.8
2	500	10^{-12}	200	100	1×10^{-5}	0.7	1.2	342.3
3	250	10^{-12}	200	100	5×10^{-5}	1.1	2.6	31.6
4	100	10^{-12}	200	100	1×10^{-3}	2.4	8.2	1.0
5	250	10^{-8}	200	100	5×10^{-5}	1.6	5.7	31.3
6	250	10^{-12}	100	50	5×10^{-5}	1.1	2.6	16.5
7	250	10^{-12}	50	25	5×10^{-5}	1.1	2.6	9.2
8	250	10^{-12}	20	20	5×10^{-5}	1.1	2.6	7.4

As follows from Table 5, for Case 2 the computational cost is approximately 12 times lower than for Case 1. This is achieved by reducing $n_{\rm layers}$ from 1000 to 500 and increasing Δt from 10^{-6} s to 10^{-5} s. The difference in predicted evaporation time and temperature in this case is rather small, at 0.7% and 1.2%, respectively. When $n_{\rm layers}$ is reduced to 250 and Δt increased to 5×10^{-5} s, maintaining the values of all the other parameters (see Case 3), the computational cost is approximately 131 times lower, while the relative errors for estimating $t_{\rm evap}$ and $\phi T_{t=5s}$ are only 1.1% and 2.6%, respectively. When $n_{\rm layers}$ was reduced to 100 and Δt increased to 10^{-3} s, maintaining the values of all the other parameters (see Case 4), the computational cost was more than 4000 times lower, while the relative errors of estimating $t_{\rm evap}$ and $\phi T_{t=5s}$ are still only 2.4% and 8.2%, respectively.

Comparing Cases 3 and 5, it can be observed that even though increasing α_{BSM} reduces the computational cost, this reduction is not significant. On the other hand, this leads to more than doubling of $\phi\tilde{T}_{t=5s}$, which brings into question the usefulness of adopting Case 5 instead of Case 3. Analysis of Cases 3, 6, 7, and 8 shows that reducing n_T and n_Y from 200 and 100 to 20 and 20, respectively, does not affect the results of calculations of droplet diameters and temperatures, but leads to a reduction in execution time from 31.6 s to 7.4 s. Note that if Surrogates 3, 7, 11 or 12, which showed the best performance in Section 6.2, were used, the execution time needed would be even lower due to the reduction in the number of components used in calculations.

7. Conclusions

A Discrete Component Model (DCM), based on the analytical solutions to the heat transfer and species diffusion equations, is used to analyse the droplet heating and evaporation of Jet A and its surrogates. The Abramzon-Sirignano model is used for the analysis of the processes in the gas phase during droplet heating and evaporation. The partial pressures of vapour species are estimated based on Raoult's law. The implementation of these models into the MFSim code opens the way to modelling the evaporation and combustion of fuel sprays.

The results achieved using the MFSim code, with new models implemented into it, are successfully validated against experimental results described in [38]. Heating and evaporation characteristics of droplets of 12 surrogates are compared with those of Jet A droplets using the same input parameters as in the experiments described in [38]. It is shown that the evaporation time of a droplet of Surrogate 12 from [30] is the closest to that predicted for a Jet A droplet, while Surrogate 3 from [24] and Surrogate 7 from [28] presented the best results when droplet evaporation rate was the target parameter. Furthermore, the maximum temperature predicted for droplets of Surrogate 11 from [29] is shown to be the closest to that predicted for a Jet A droplet. Surrogates 3, 7, 11 or 12 are recommended depending on the target parameters considered.

Sensitivity analysis of various numerical parameters was conducted, which included: the number of concentric layers used to discretise the droplet volume, the absolute accuracy of the bisection method used for finding the eigenvalues in the analytical solutions for temperature and species mass fractions, the number of terms in the series for temperature and species mass fractions, and the duration of time steps used in simulations. For the investigated cases, it is shown that: the number of layers should not be lower than 250; using a less restrictive accuracy for finding the eigenvalues does not significantly reduce the computational cost and results in greater deviations; and the number of terms of the series for temperature and species mass fractions can be reduced from 200 to 20 without affecting the accuracy of calculations. Additionally, it is observed that droplet temperature is more sensitive than evaporation time to variations in the analysed numerical parameters. Finally, it is demonstrated that the best compromise between accuracy and CPU requirement is achieved for the combination of numerical parameters used in Case 8 shown in Table 5. This combination of numerical parameters, $n_{\text{layers}} = 250$, $\alpha_{\text{BSM}} = 10^{-12}$, $n_T = 20$, $n_Y = 20$ and $\Delta t = 5 \times 10^{-5}$, can also be used to study other multicomponent droplets.

Conflict of interest

The authors declare that there is no conflict of interest.

Acknowledgment

The authors are grateful for the financial and technical support received from Petróleo Brasileiro S.A. (Petrobras) and the National Counsel of Technological and Scientific Development (CNPq), which supported A. P. Pinheiro (responsible for analysis of the background of the problem, formulation of the problem, development of the numerical code, analysis of the results and preparation of the first draft of the paper), F. L. Sacomano Filho and J. M. Vedovotto (who both contributed to the formulation of the problem and analysis of the results).

The authors are also grateful for financial support received from the Royal Society (UK) (Grant no. IEC 192007) and the UKRI Future Leaders Fellowship (Grant no. MR/T043326/1), which supported O. Rybdylova (who contributed to the development of the numerical code), and the Russian Science Foundation (Grant 21-19-00876), which supported I. A. Zubrilin (responsible for the selection of Jet A surrogates) and S. S. Sazhin (who contributed to the development of the model, analysis of the results and preparation of the text of the paper).

References

[1] G. Eckel, J. Grohmann, L. Cantu, N. Slavinskaya, T. Kathrotia, M. Rachner, P. Le Clercq, W. Meier, M. Aigner, LES of a swirl-stabilized kerosene spray flame with a multi-component vaporization model and detailed chemistry, Combustion and Flame 207 (2019) 134–152. doi:10.1016/j.combustflame.2019.05.011.

[2] W. A. Sirignano, Fluid Dynamics and Transport of Droplets and Sprays, 2nd Edition, Cambridge University Press, 2010. doi:10.1017/CBO9780511806728.

[3] S. S. Sazhin, Droplets and Sprays, Springer, 2014.

[4] S. S. Sazhin, Modelling of fuel droplet heating and evaporation: Recent results and unsolved problems, Fuel 196 (2017) 69–101. doi:10.1016/j.fuel.2017.01.048.

[5] S. S. Sazhin, M. Al Qubeissi, R. Nasiri, V. M. Gun'ko, A. E. Elwardany, F. Lemoine, F. Grisch, M. R. Heikal, A multi-dimensional quasi-discrete model for the analysis of diesel fuel droplet heating and evaporation, Fuel 129 (2014) 238–266. doi:10.1016/j.fuel.2014.03.028.

[6] J. Baumi, C. M. Bertosse, C. L. B. Guedes, Aviation fuels and biofuels, in: M. A. Qubeissi, A. El-kharouf, H. S. Soyhan (Eds.), Renewable Energy, IntechOpen, Rijeka, 2020, Ch. 12. doi:10.5772/intechopen.89397.

[7] M. Burger, R. Schmehl, K. Prommersberger, O. Schfer, R. Koch, S. Wittig, Droplet evaporation modeling by the distillation curve model: accounting for kerosene fuel and elevated pressures, International Journal of Heat and Mass Transfer 46 (23) (2003) 4403–4412. doi:10.1016/S0017-9310(03)00286-2.

[8] W. L. H. Hallett, N. V. Legault, Modelling biodiesel droplet evaporation using continuous thermodynamics, Fuel 90 (3) (2011) 1221–1228. doi:10.1016/j.fuel.2010.11.035.

[9] M. Al Qubeissi, N. Al-Esawi, S. S. Sazhin, Auto-selection of quasi-components/components in the multi-dimensional quasi-discrete model, Fuel 294 (2021) 120245. doi:10.1016/j.fuel.2021.120245.

[10] L. Poulton, O. Rybdylova, I. A. Zubrilin, S. G. Matveev, N. I. Gurakov, M. Al Qubeissi, N. Al-Esawi, T. Khan, V. M. Gun'ko, S. S. Sazhin, Modelling of multi-component kerosene and surrogate fuel droplet heating and evaporation characteristics: A comparative analysis, Fuel 269 (2020) 117115. doi:10.1016/j.fuel.2020.117115.

[11] K. Lissitsyna, S. Huertas, L. C. Quintero, L. M. Polo, PIONA analysis of kerosene by comprehensive two-dimensional gas chromatography coupled to time of flight mass spectrometry, Fuel 116 (2014) 716–722. doi:10.1016/j.fuel.2013.07.077.

[12] M. R. Pivello, M. M. Villar, R. Serfaty, A. M. Roma, A. da Silveira Neto, A fully adaptive front tracking method for the simulation of two phase flows, International Journal of Multiphase Flow 58 (2014) 72–82. doi:10.1016/j.ijmultiphaseflow.2013.08.009.

[13] L. P. Castro, A. P. Pinheiro, V. Vilela, G. M. Magalhães, R. Serfaty, J. M. Vedovotto, Implementation of a hybrid lagrangian filtered density functionlarge eddy simulation methodology in a dynamic adaptive mesh refinement environment, Physics of Fluids 33 (4) (2021) 045126. doi:10.1063/5.0045873.

[14] A. P. Pinheiro, J. M. Vedovoto, Evaluation of droplet evaporation models and the incorporation of natural convection effects, Flow, Turbulence and Combustion 102 (3) (2019) 537–558. doi:10.1007/s10494-018-9973-8.

[15] A. P. Pinheiro, J. M. Vedovoto, A. da Silveira Neto, B. G. van Wachem, Ethanol droplet evaporation: Effects of ambient temperature, pressure and fuel vapor concentration, International Journal of Heat and Mass Transfer 143 (2019) 118472. doi:10.1016/j.ijheatmasstransfer.2019.118472.

[16] B. Abramzon, W. A. Sirignano, Droplet vaporization model for spray combustion calculations, International Journal of Heat and Mass Transfer 32 (9) (1989) 1605–1618. doi:10.1016/0017-9310(89)90043-4.

[17] G. Continillo, W. Sirignano, Numerical study of multicomponent fuel spray flame propagation in a spherical closed volume, Symposium (International) on Combustion 22 (1989) 1941–1949. doi:10.1016/S0082-0784(89)80209-7.

[18] G. L. Hubbard, V. E. Denny, A. F. Mills, Droplet evaporation: Effects of transients and variable properties, International Journal of Heat and Mass Transfer 18 (9) (1975) 1003–1008.

[19] M. C. Yuen, L. W. Chen, On drag of evaporating liquid droplets, Combustion Science and Technology 14 (4-6) (1976) 147–154.

[20] O. Rybdylova, M. Al Qubeissi, M. Braun, C. Crua, J. Manin, L. M. Pickett, G. De Sercey, E. M. Sazhina, S. S. Sazhin, M. Heikal, A model for droplet heating and its implementation into ANSYS Fluent, International Communications in Heat and Mass Transfer 76 (2016) 265–270. doi:10.1016/j.icheatmasstransfer.2016.05.032.

[21] C. Law, W. Sirignano, Unsteady droplet combustion with droplet heating - II: Conduction limit, Combustion and Flame 28 (1977) 175–186. doi:10.1016/0010-2180(77)90023-2.

[22] J. Kiusalaas, Numerical Methods in Engineering with Python 3, 3rd Edition, Cambridge University Press, 2013. doi:10.1017/CBO9781139523899.

[23] P. Vozka, D. Vrtiška, P. Šimaček, G. Kilaz, Impact of alternative fuel blending components on fuel composition and properties in blends with Jet A, Energy & Fuels 33 (4) (2019) 3275–3289. doi:10.1021/acs.energyfuels.9b00105.

[24] S. Dooley, S. H. Won, M. Chaos, J. Heyne, Y. Ju, F. L. Dryer, K. Kumar, C.-J. Sung, H. Wang, M. A. Oehlschlaeger, R. J. Santoro, T. A. Litzinger, A jet fuel surrogate formulated by real fuel properties, Combustion and Flame 157 (12) (2010) 2333–2339. doi:10.1016/j.combustflame.2010.07.001.

[25] M. L. Huber, E. W. Lemmon, T. J. Bruno, Surrogate mixture models for the thermophysical properties of aviation fuel Jet-A, Energy & Fuels 24 (6) (2010) 3565–3571. doi:10.1021/ef700562c.

[26] S. Dooley, S. H. Won, J. Heyne, T. I. Farouk, Y. Ju, F. L. Dryer, K. Kumar, X. Hui, C.-J. Sung, H. Wang, M. A. Oehlschlaeger, V. Iyer, S. Iyer, T. A. Litzinger, R. J. Santoro, T. Malewicki, K. Brezinsky, The experimental evaluation of a methodology for surrogate fuel formulation to emulate gas phase combustion kinetic phenomena, Combustion and Flame 159 (4) (2012) 1444–1466. doi:10.1016/j.combustflame.2011.11.002.

[27] D. Kim, J. Martz, A. Violi, A surrogate for emulating the physical and chemical properties of conventional jet fuel, Combustion and Flame 161 (6) (2014) 1489–1498. doi:10.1016/j.combustflame.2013.12.015.

[28] J. Yu, Y. Ju, X. Gou, Surrogate fuel formulation for oxygenated and hydrocarbon fuels by using the molecular structures and functional groups, Fuel 166 (2016) 211–218. doi:10.1016/j.fuel.2015.10.085.

[29] S. H. Won, F. M. Haas, S. Dooley, T. Edwards, F. L. Dryer, Reconstruction of chemical structure of real fuel by surrogate formulation based upon

combustion property targets, Combustion and Flame 183 (2017) 39–49. doi:10.1016/j.combustflame.2017.04.032.

[30] A. G. Abdul Jameel, N. Naser, A.-H. Emwas, S. M. Sarathy, Surrogate formulation for diesel and jet fuels using the minimalist functional group (MFG) approach, Proceedings of the Combustion Institute 37 (4) (2019) 4663–4671. doi:10.1016/j.proci.2018.09.035.

[31] D. G. Goodwin, H. K. Moffat, R. L. Speth, Cantera: An object-oriented software toolkit for chemical kinetics, thermodynamics, and transport processes, http://www.cantera.org, Version 2.2.1 (2016).

[32] M. Sanjosé, Evaluation de la méthode Euler-Euler pour la simulation aux grandes échelles des chambres à carburant liquide, Ph.D. thesis, Institut National Polytechnique de Toulouse - INPT (2009).

[33] C. Yaws, Yaws' Handbook of Thermodynamic and Physical Properties of Chemical Compounds, Knovel, 2003.

[34] C. Yaws, (Eds.), Thermophysical properties of chemicals and hydrocarbons, William Andrew, Norwich, NY, 2008.

[35] C. Yaws, (Eds.), Transport properties of chemicals and hydrocarbons: viscosity, thermal conductivity, and diffusivity of C1 to C100 organics and Ac to Zr inorganic, William Andrew, 2009.

[36] R. B. Bird, E. N. Lightfoot, W. E. Stewart, Transport Phenomena, Wiley, 2002.

[37] C. M. Silva, H. Liu, E. A. Macedo, Models for self-diffusion coefficients of dense fluids, including hydrogen-bonding substances, Chemical Engineering Science 53 (13) (1998) 2423–2429. doi:10.1016/S0009-2509(98)00037-2.

[38] F. Wang, R. Liu, M. Li, J. Yao, J. Jin, Kerosene evaporation rate in high temperature air stationary and convective environment, Fuel 211 (2018) 582–590. doi:10.1016/j.fuel.2017.08.062.

[39] H. Ghassemi, S. W. Baek, Q. S. Khan, Experimental study on evaporation of kerosene droplets at elevated pressures and temperatures, Combustion Science and Technology 178 (9) (2006) 1669–1684. doi:10.1080/00102200600582392.

[40] Q. Khan, S. W. Baek, S. Y. Lee, Effect of droplet initial diameter on droplet vaporization regimes for kerosene fuel droplet, in: 45th AIAA Aerospace Sciences Meeting and Exhibit, 2007, p. 1181.

[41] I. Javed, S. W. Baek, K. Waheed, G. Ali, S. O. Cho, Evaporation characteristics of kerosene droplets with dilute concentrations of ligand-protected aluminum nanoparticles at elevated temperatures, Combustion and Flame 160 (12) (2013) 2955–2963. doi:10.1016/j.combustflame.2013.07.007.

[42] J. Yoon, S. W. Baek, Droplet evaporation behavior of kerosene/nano-aluminum fuels at high pressure environment, International Journal of Material and Mechanical Engineering 4 (2015) 44–49. doi:10.14355/ijmme.2015.04.007.

[43] O. Rybdylova, L. Poulton, M. Al Qubeissi, A. E. Elwardany, C. Crua, T. Khan, S. S. Sazhin, A model for multi-component droplet heating and evaporation and its implementation into ANSYS Fluent, International Communications in Heat and Mass Transfer 90 (2018) 29–33. doi:10.1016/j.icheatmasstransfer.2017.10.018.

Modelling of aviation kerosene droplet heating and evaporation using complete fuel composition and surrogates

Supplementary Material

1. Thermodynamic and transport properties database

The transport and thermodynamic properties of the individual Jet A components used, based on the tabulated data collected from [1, 2, 3], are presented in the following section. In Section 2, the transport and thermodynamic properties of the components used in Jet A surrogates are presented. The transport and thermodynamic properties are presented in SI units, unless the unit is specified.

1.1. Jet A properties

The properties here presented are valid for the following components, with n representing the number of carbon atoms of each component:

- n-paraffins (C_nH_{2n+2}) for $7 \leqslant n \leqslant 18$;
- iso-paraffins (C_nH_{2n+2}) for $7 \leqslant n \leqslant 18$;
- monocycloparaffins (C_nH_{2n}) for $7 \leqslant n \leqslant 17$;
- dicycloparaffins (C_nH_{2n-2}) for $8 \leqslant n \leqslant 15$;
- alkylbenzenes (C_nH_{2n-6}) for $6 \leqslant n \leqslant 17$;
- cycloaromatics (C_nH_{2n-8}) for $9 \leqslant n \leqslant 15$;
- alkylnaphthalenes (C_nH_{2n-12}) for $10 \leqslant n \leqslant 15$.

1.1.1. Critical temperature and pressure

Following [4] and using data provided in [2], the dependencies of critical temperature and pressure on carbon number are approximated by the following equations:

$$T_{\mathrm{cr}}(n) = A_{\mathrm{cr}} + B_{\mathrm{cr}}n + C_{\mathrm{cr}}n^2 + D_{\mathrm{cr}}n^3, \tag{1}$$

$$p_{\mathrm{cr}}(n) = A_{\mathrm{cr}} + B_{\mathrm{cr}}n + C_{\mathrm{cr}}n^2 + D_{\mathrm{cr}}n^3, \tag{2}$$

where p_{cr} is given in bar and the coefficients A_{cr}, B_{cr}, C_{cr} and D_{cr} for each hydrocarbon group to calculate both critical temperature and pressure are:

Table 1: Coefficients to calculate critical temperature based on Eq. 1.

Coef	n-par	iso-par	monocyclo	dicyclo
A_{cr}	263.57832168	292.10720280	29.09477525	-320.64867965
B_{cr}	51.40631961	41.58990417	128.15485043	190.61380231
C_{cr}	-1.89891220	-1.18311577	-7.75925408	-11.29790043
D_{cr}	0.02973323	0.01732971	0.17323815	0.22717172

Coef	alkyb	cycloa	alkylnaph
A_{cr}	451.04119991	-111.160952	445.642857
B_{cr}	9.75417786	167.850397	36.9344312
C_{cr}	1.92963148	-11.4427381	-0.711031746
D_{cr}	-0.07296685	0.29305556	0.00453704

Table 2: Coefficients to calculate critical pressure based on Eq. 2.

Coef	n-par	iso-par	monocyclo	dicyclo
A_{cr}	50.97492507	44.16799201	56.96146853	41.43409091
B_{cr}	-4.44716302	-3.09357402	-2.18197747	0.71171717
C_{cr}	0.16675547	0.10287324	-0.11116550	-0.36636364
D_{cr}	-0.00206553	-0.00150479	0.00626651	0.01479798

Coef	alkyb	cycloa	alkylnaph
A_{cr}	117.09889777	38.57904762	71.12714286
B_{cr}	-16.50622156	5.78865079	4.39328042
C_{cr}	0.96297869	-0.88821429	-1.20222222
D_{cr}	-0.02007382	0.02861111	0.04592593

1.1.2. Liquid density

The following approximations are based on droplet average temperatures. They are assumed to be valid until the vicinity of the liquid component critical temperatures are reached. Following [4] and using data provided in [2], the dependency of liquid density on carbon number and droplet average temperature is approximated by the following equation:

$$\rho_l(T) = 1000 A_\rho B_\rho^{-\left(1-\frac{T}{T_{\mathrm{cr}}}\right)^{C_\rho}}, \tag{3}$$

where A_ρ, B_ρ and C_ρ are approximated using the following expressions:

for n-paraffins,

$$\begin{cases} A_\rho = -3.651 \times 10^{-5} n^3 + 1.23322 \times 10^{-3} n^2 - 0.01233966 n + 0.27108194, \\ B_\rho = -1.308 \times 10^{-5} n^3 + 5.2495 \times 10^{-4} n^2 - 7.41829 \times 10^{-3} n + 0.29111626, \\ C_\rho = -3.3428 \times 10^{-4} n^3 + 0.01169429 n^2 - 0.12576357 n + 0.70298720, \\ C_\rho = 0.27348, \quad \text{if} \quad n = 14. \end{cases} \tag{4}$$

for iso-paraffins,

$$\begin{cases} A_\rho = -4.56 \times 10^{-6} n^3 + 5.956 \times 10^{-5} n^2 + 1.52591 \times 10^{-3} n + 0.22380305, \\ A_\rho = 0.23379, \quad \text{if} \quad n = 18, \\ B_\rho = -1.389 \times 10^{-5} n^3 + 5.9426 \times 10^{-4} n^2 - 8.56097 \times 10^{-3} n + 0.30516675, \\ B_\rho = 5.075 \times 10^{-5} n^3 - 1.80925 \times 10^{-3} n^2 + 0.01873450 n + 0.2019320, \\ \text{if} \quad n = 8, 9, 12, 18, \\ C_\rho = -3.56167 \times 10^{-3} n^3 + 0.096530 n^2 - 0.85372833 n + 2.746780, \quad \text{if} \quad n \leqslant 10, \\ C_\rho = 0.28571, \quad \text{if} \quad n \geqslant 11. \end{cases} \tag{5}$$

for monocycloparaffins,

$$\begin{cases} A_\rho = -1.708 \times 10^{-5} n^3 + 4.7114 \times 10^{-4} n^2 - 2.21842 \times 10^{-3} n + 0.27093140, \\ B_\rho = -1.4619 \times 10^{-4} n^3 + 4.98771 \times 10^{-3} n^2 - 0.0524475 n + 0.44174696, \\ B_\rho = 1.9250 \times 10^{-4} n^2 - 4.19250 \times 10^{-3} n + 0.333120, \quad \text{if} \quad n = 14, 16, 17, \\ C_\rho = 0.28571. \end{cases} \tag{6}$$

for dicycloparaffins,

$$\begin{cases} A_\rho = -3.705 \times 10^{-5} n^3 + 4.8848 \times 10^{-4} n^2 + 5.33995 \times 10^{-3} n + 0.21543407, \\ B_\rho = -1.0292 \times 10^{-4} n^3 + 3.62171 \times 10^{-3} n^2 - 0.04138827 n + 0.4190520, \\ B_\rho = 0.27581, \quad \text{if} \quad n = 13, \\ C_\rho = 0.28571. \end{cases} \tag{7}$$

for alkylbenzenes,

$$\begin{cases} A_\rho = -9.714 \times 10^{-5} n^3 + 3.62102 \times 10^{-3} n^2 - 0.04655698 n + 0.47235423, \\ B_\rho = -6.912 \times 10^{-10} n^3 + 2.41783 \times 10^{-3} n^2 - 0.02853582 n + 0.36699367, \\ C_\rho = 1.8244 \times 10^{-4} n^3 - 5.84519 \times 10^{-3} n^2 + 0.05870678 n + 0.10448834, \\ C_\rho = -0.0151250 n^2 + 0.4137250 n - 2.501350, \quad \text{if} \quad n = 13, 14, 15. \end{cases} \tag{8}$$

for cycloaromatics,

$$\begin{cases} A_\rho = -1.250 \times 10^{-4} n^3 + 4.95940 \times 10^{-3} n^2 - 0.068848607 n + 0.61540095, \\ B_\rho = 6.11 \times 10^{-6} n^3 + 1.5298 \times 10^{-4} n^2 - 7.25956 \times 10^{-3} n + 0.30978857, \\ C_\rho = 0.28571, \\ C_\rho = -0.034530 n + 0.6130, \quad \text{if} \quad n = 9, 10. \end{cases} \tag{9}$$

for alkylnaphthalenes,

$$\begin{cases} A_\rho = -3.62 \times 10^{-6} n^3 + 3.4528 \times 10^{-4} n^2 - 0.01143223 n + 0.39374717, \\ A_\rho = 0.2719, \quad \text{if} \quad n = 11, \\ B_\rho = -4.2796 \times 10^{-4} n^3 + 0.01404540 n^2 - 0.14220378 n + 0.66715857, \\ C_\rho = -2.620 \times 10^{-3} n^3 + 0.097870 n^2 - 1.203960 n + 5.14560, \\ C_\rho = 0.28571, \quad \text{if} \quad n = 13, 15. \end{cases} \tag{10}$$

1.1.3. Liquid dynamic viscosity

The following approximations are based on droplet average temperatures. They are assumed to be valid until the vicinity of the liquid component critical temperatures are reached. Following [4] and using data provided in [3], the dependency of liquid dynamic viscosity on carbon number and droplet average temperature is approximated by the following equation:

$$\mu_l(T) = 0.001 \times 10^{A_v + \frac{B_v}{T} + C_v T + D_v T^2}, \tag{11}$$

where the coefficients A_v, B_v, C_v and D_v for each hydrocarbon group are:

for n-paraffins,

$$\begin{cases} A_\mu = 1.6635 \times 10^{-3} n^3 - 0.052863 n^2 + 0.21103 n - 4.8442, \\ B_\mu = -0.24372 n^3 + 6.1103 n^2 + 49.962 n + 191.42, \\ C_\mu = -6.8753 \times 10^{-6} n^3 + 2.5868 \times 10^{-4} n^2 - 2.7814 \times 10^{-3} n + 0.021678, \\ D_\mu = 1.2888 \times 10^{-8} n^3 - 5.0968 \times 10^{-7} n^2 + 6.5990 \times 10^{-6} n - 4.0175 \times 10^{-5}. \end{cases} \tag{12}$$

for iso-paraffins,

$$\begin{cases} A_\mu = 0.012873 n^3 - 0.49949 n^2 + 6.2260 n - 30.166, \\ B_\mu = -1.3323 n^3 + 51.923 n^2 - 618.43 n + 3.1441 E3, \\ C_\mu = -3.5487 \times 10^{-5} n^3 + 1.3934 \times 10^{-3} n^2 - 0.017960 n + 0.085316, \\ D_\mu = 3.4619 \times 10^{-8} n^3 - 1.3814 \times 10^{-6} n^2 + 1.8379 \times 10^{-5} n - 8.9821 \times 10^{-5}. \end{cases} \tag{13}$$

for monocycloparaffins,

$$\begin{cases} A_\mu = 8.6111 \times 10^{-3} n^3 - 0.33451 n^2 + 3.9745 n - 20.158, \\ B_\mu = -1.1679 n^3 + 44.088 n^2 - 474.62 n + 2.5092 E3, \\ C_\mu = -2.3440 \times 10^{-5} n^3 + 9.2128 \times 10^{-4} n^2 - 0.011445 n + 0.054663, \\ D_\mu = 2.2707 \times 10^{-8} n^3 - 9.0395 \times 10^{-7} n^2 + 1.1655 \times 10^{-5} n - 5.6371 \times 10^{-5}. \end{cases} \tag{14}$$

for dicycloparaffins,

$$\begin{cases} A_\mu = 0.072794 n^3 - 1.9886 n^2 + 16.419 n - 42.703, \\ B_\mu = -15.668 n^3 + 463.60 n^2 - 4.3255 E3 n + 1.3464 E4, \\ C_\mu = -8.6777 \times 10^{-5} n^3 + 1.8914 \times 10^{-3} n^2 - 8.5977 \times 10^{-3} n - 8.4313 \times 10^{-3}, \\ D_\mu = -1.1165 \times 10^{-7} n^3 + 3.9247 \times 10^{-6} n^2 - 4.5025 \times 10^{-5} n + 1.6352 \times 10^{-4}. \end{cases} \tag{15}$$

for alkylbenzenes,

$$\begin{cases} A_\mu = -0.041760 n^3 + 1.3069 n^2 - 13.448 n + 38.038, \\ B_\mu = 2.2210 n^3 - 66.855 n^2 + 744.21 n - 1.7787 E3, \\ C_\mu = 1.0143 \times 10^{-4} n^3 - 3.1853 \times 10^{-3} n^2 + 0.032736 n - 0.096135, \\ D_\mu = -9.7759 \times 10^{-8} n^3 + 3.0771 \times 10^{-6} n^2 - 3.1220 \times 10^{-5} n + 8.9907 \times 10^{-5}. \end{cases} \tag{16}$$

for cycloaromatics,

$$\begin{cases} A_\mu = 5.5000 \times 10^{-3} n^3 - 0.44859 n^2 + 8.6641 n - 53.134, \\ B_\mu = 4.2774 n^3 - 105.25 n^2 + 623.23 n + 1.1654 E3, \\ C_\mu = -1.5417 \times 10^{-5} n^3 + 1.0300 \times 10^{-3} n^2 - 0.018711 n + 0.10910, \\ D_\mu = -3.8333 \times 10^{-8} n^3 + 1.0913 \times 10^{-6} n^2 - 8.9503 \times 10^{-6} n + 1.1289 \times 10^{-5}. \end{cases} \tag{17}$$

for alkylnaphthalenes,

$$\begin{cases} A_\mu = 2.7433n^3 - 95.336n^2 + 1.1001E3n - 4.2213E3, \\ B_\mu = -474.32n^3 + 1.6475E4n^2 - 1.8997E5n + 7.2836E5, \\ C_\mu = -5.9552 \times 10^{-3}n^3 + 0.20671n^2 - 2.3827n + 9.1302, \\ D_\mu = 4.1097 \times 10^{-6}n^3 - 1.4245 \times 10^{-4}n^2 + 1.6398 \times 10^{-3}n - 6.2761 \times 10^{-3}. \end{cases} \tag{18}$$

1.1.4. Liquid thermal conductivity

The following approximations are based on droplet average temperatures. They are assumed to be valid until the vicinity of the liquid component critical temperatures are reached. Following [4] and using data provided in [3], the dependency of liquid thermal conductivity on carbon number and droplet average temperature is approximated by the following equation:

$$k_l(T) = \left(A_k + B_k T + C_k T^2\right). \tag{19}$$

where the coefficients A_k, B_k and C_k for each hydrocarbon group are:

for n-paraffins,

$$\begin{cases} A_k = -1.28427 \times 10^{-5}n^3 - 5.98159 \times 10^{-6}n^2 + 5.96748 \times 10^{-3}n + 1.80190 \times 10^{-1}, \\ A_k = -3.51286 \times 10^{-5}n^3 + 1.65484 \times 10^{-3}n^2 - 2.44423 \times 10^{-2}n + 3.11264 \times 10^{-1}, \\ \quad \text{if} \quad n = 9, 13, 14, 15, 16, \\ B_k = 2.81312 \times 10^{-8}n^3 + 1.9869 \times 10^{-6}n^2 - 5.84508 \times 10^{-5}n + 7.34781 \times 10^{-6}, \\ B_k = -2.0 \times 10^{-4}, \quad \text{if} \quad n = 9, 13, 14, 15, 16, \\ C_k = -7.45277 \times 10^{-10}n^3 + 1.97325 \times 10^{-8}n^2 - 1.10986 \times 10^{-7}n - 1.18479 \times 10^{-8}, \\ C_k = 0, \quad \text{if} \quad n = 13, 14, 15, 16. \end{cases} \tag{20}$$

for iso-paraffins,

$$\begin{cases} A_k = 5.89225589 \times 10^{-6}n^3 - 1.42463092 \times 10^{-4}n^2 + 2.41178451 \times 10^{-3}n + \\ +1.75310490 \times 10^{-1}, \\ B_k = -2.5 \times 10^{-4}, \\ B_k = -2.57 \times 10^{-4}, \quad \text{if} \quad n = 8, \\ C_k = 0. \end{cases} \tag{21}$$

for monocycloparaffins,

$$\begin{cases} A_k = 5.83916084 \times 10^{-5} n^3 - 2.00268065 \times 10^{-3} n^2 + 1.65643357 \times 10^{-2} n + \\ +1.44828205 \times 10^{-1}, \\ B_k = -7.81721057 \times 10^{-8} n^3 + 2.44378788 \times 10^{-6} n^2 - 1.52993687 \times 10^{-5} n - \\ -1.84743007 \times 10^{-4}, \\ C_k = 0. \end{cases} \quad (22)$$

for dicycloparaffins,

$$\begin{cases} A_k = -1.38333333 \times 10^{-3} n^3 + 4.29440476 \times 10^{-2} n^2 - 4.426750 \times 10^{-1} n + 1.70659286, \\ A_k = 2.17 \times 10^{-1}, \quad \text{if} \quad n = 15, \\ B_k = -2.5 \times 10^{-4}, \\ B_k = -6.18 \times 10^{-6} n^2 + 1.63919 \times 10^{-4} n - 1.16888 \times 10^{-3}, \quad \text{if} \quad n = 10, 13, 14, \\ C_k = 0. \end{cases} \quad (23)$$

for alkylbenzenes,

$$\begin{cases} A_k = 5.82390601 \times 10^{-5} n^3 - 1.76280647 \times 10^{-3} n^2 + 1.81168242 \times 10^{-2} n + \\ +1.26657757 \times 10^{-1}, \\ A_k = 2.1 \times 10^{-1}, \quad \text{if} \quad n = 7, \\ B_k = 4.53152174 \times 10^{-7} n^3 - 2.96894410 \times 10^{-7} n^2 - 1.21991693 \times 10^{-4} n + \\ +5.64151957 \times 10^{-4}, \\ B_k = -2.86 \times 10^{-4}, \quad \text{if} \quad n = 7, \\ B_k = -2.0 \times 10^{-4}, \quad \text{if} \quad 13 \leqslant n \leqslant 17, \\ C_k = 3.44898148 \times 10^{-9} n^3 - 1.01939849 \times 10^{-7} n^2 + 1.00913420 \times 10^{-6} n - \\ -3.30045979 \times 10^{-6}, \\ C_k = 0, \quad \text{if} \quad 12 \leqslant n \leqslant 17. \end{cases} \quad (24)$$

for cycloaromatics,

$$\begin{cases} A_k = 3.04347826 \times 10^{-4} n^3 - 1.18446170 \times 10^{-2} n^2 + 1.54743789 \times 10^{-1} n - \\ -4.65067495 \times 10^{-1}, \\ A_k = 1.50 \times 10^{-1}, \quad \text{if} \quad n = 10, \\ B_k = -2.5 \times 10^{-4}, \\ B_k = 1.2104 \times 10^{-4} n - 1.277097 \times 10^{-3}, \quad \text{if} \quad n = 9, 10, \\ C_k = 0. \end{cases} \quad (25)$$

for alkylnaphthalenes,

$$\begin{cases} A_k = 5.86792453 \times 10^{-4} n^3 - 2.36010782 \times 10^{-2} n^2 + 3.17659299 \times 10^{-1} n - 1.21404636, \\ A_k = 1.63 \times 10^{-1}, \quad \text{if} \quad n = 11, \\ B_k = -2.5 \times 10^{-4}, \\ B_k = 2.889 \times 10^{-5} n - 4.289 \times 10^{-4}, \quad \text{if} \quad n = 10, 11, \\ C_k = 0. \end{cases} \tag{26}$$

1.1.5. Liquid specific heat capacity

The following approximations are based on droplet average temperatures. They are assumed to be valid until the vicinity of the liquid component critical temperatures are reached. Following [4] and using data provided in [1], the dependency of liquid specific heat capacity on carbon number and droplet average temperature is approximated by the following equation:

$$c_l(T) = \frac{1000}{M(n)} \left(A_c + B_c T + C_c T^2 + D_c T^3 \right), \tag{27}$$

where $M(n)$ is the component molar mass and the coefficients A_c, B_c, C_c and D_c for each hydrocarbon group are:

for n-paraffins,

$$\begin{cases} A_c = 0.13603069 n^3 - 4.07475758 n^2 + 38.32630264 n - 22.56629371, \\ B_c = -3.5284 \times 10^{-4} n^3 + 8.21387 \times 10^{-3} n^2 + 0.13820726 n - 0.22870, \\ C_c = 9.91712 \times 10^{-8} n^3 + 1.02012 \times 10^{-5} n^2 - 5.90184 \times 10^{-4} n + 4.16866 \times 10^{-4}, \\ D_c = -4.87995 \times 10^{-10} n^3 + 9.55370 \times 10^{-9} n^2 + 1.3320 \times 10^{-7} n + 3.04028 \times 10^{-6}. \end{cases} \tag{28}$$

for iso-paraffins,

$$\begin{cases} A_c = -2.347009 \times 10^{-2} n^3 + 0.31530003 n^2 + 18.49326762 n - 21.46292907, \\ B_c = 6.5180 \times 10^{-4} n^3 - 2.267697 \times 10^{-2} n^2 + 0.34579880 n - 0.85354515, \\ C_c = -1.34132 \times 10^{-6} n^3 + 4.32455 \times 10^{-5} n^2 - 6.07901 \times 10^{-4} n + 3.56658 \times 10^{-4}, \\ D_c = 8.85496 \times 10^{-10} n^3 - 2.40940 \times 10^{-8} n^2 + 2.60783 \times 10^{-7} n + 2.45139 \times 10^{-6}. \end{cases} \tag{29}$$

for monocycloparaffins,

$$\begin{cases} A_c = 0.10425117n^3 - 4.04246037n^2 + 63.74764744n - 173.940669, \\ B_c = -2.13813 \times 10^{-3}n^3 + 8.881317 \times 10^{-2}n^2 - 1.05086735n + 4.23265268, \\ C_c = 5.13963 \times 10^{-6}n^3 - 2.09951 \times 10^{-4}n^2 + 2.51306 \times 10^{-3}n - 0.0103186, \\ D_c = -4.9857 \times 10^{-9}n^3 + 2.01118 \times 10^{-7}n^2 - 2.44869 \times 10^{-6}n + 1.06439 \times 10^{-5}. \end{cases} \tag{30}$$

for dicycloparaffins,

$$\begin{cases} A_c = -1.78825505n^3 + 62.94041234n^2 - 698.63173088n + 2628.71217965, \\ B_c = 0.01080833n^3 - 0.37819048n^2 + 4.330275n - 15.62234286, \\ C_c = -2.78888 \times 10^{-5}n^3 + 9.72118 \times 10^{-4}n^2 - 1.10501 \times 10^{-2}n + 3.95482 \times 10^{-2}, \\ D_c = 2.57278 \times 10^{-8}n^3 - 8.87394 \times 10^{-7}n^2 + 9.94176 \times 10^{-6}n - 3.44554 \times 10^{-5}. \end{cases} \tag{31}$$

for alkylbenzenes,

$$\begin{cases} A_c = 0.73529552n^3 - 26.59176035n^2 + 325.16134562n - 1170.11013398, \\ B_c = -2.65776 \times 10^{-3}n^3 + 0.11104252n^2 - 1.40254946n + 6.10534237, \\ C_c = 6.72440 \times 10^{-6}n^3 - 2.82790 \times 10^{-4}n^2 + 3.64120 \times 10^{-3}n - 1.62253 \times 10^{-2}, \\ D_c = -6.09978 \times 10^{-9}n^3 + 2.54403 \times 10^{-7}n^2 - 3.26094 \times 10^{-6}n + 1.51168 \times 10^{-5}. \end{cases} \tag{32}$$

for cycloaromatics,

$$\begin{cases} A_c = 1.318n^3 - 50.82504762n^2 + 663.61557143n - 2726.1422381, \\ B_c = -0.01116667n^3 + 0.42945595n^2 - 5.36197262n + 22.2708333, \\ C_c = 3.01617 \times 10^{-5}n^3 - 1.15686 \times 10^{-3}n^2 + 1.44459 \times 10^{-2}n - 5.99228 \times 10^{-2}, \\ D_c = -2.85694 \times 10^{-8}n^3 + 1.08908 \times 10^{-6}n^2 - 1.35182 \times 10^{-5}n + 5.60791 \times 10^{-5}. \end{cases} \tag{33}$$

for alkylnaphthalenes,

$$\begin{cases} A_c = 4.41637963n^3 - 181.03675397n^2 + 2483.50515212n - 11177.81671428, \\ B_c = -0.03188704n^3 + 1.30490675n^2 - 17.64329907n + 79.36332857, \\ C_c = 5.94756 \times 10^{-5}n^3 - 2.46284 \times 10^{-3}n^2 + 3.36634 \times 10^{-2}n - 1.53081 \times 10^{-1}, \\ D_c = -3.88611 \times 10^{-8}n^3 + 1.62467 \times 10^{-6}n^2 - 2.23411 \times 10^{-5}n + 1.02473 \times 10^{-4}. \end{cases} \tag{34}$$

1.1.6. Latent heat of evaporation

Following [4] and using data provided in [2], the dependency of latent heat of evaporation on carbon number and droplet surface temperature is approximated by the following equation:

$$L = \frac{A_L(1-T_r)^{B_L}}{M(n)} \times 10^6, \tag{35}$$

where $M(n)$ is the component molar mass, $T_r = T/T_{\rm cr}$ and the coefficients A_L and B_L for each hydrocarbon group are:

for n-paraffins,

$$\begin{cases} A_L = 0.02371026n^3 - 0.93664206n^2 + 16.77309084n - 29.36052817, \\ B_L = 4.891 \times 10^{-5}n^3 - 1.69720 \times 10^{-3}n^2 + 0.02395828n + 0.27914689, \\ B_L = 6.0 \times 10^{-3}n + 0.391, \quad \text{if} \quad n = 8, 10. \end{cases} \tag{36}$$

for iso-paraffins,

$$\begin{cases} A_L = 0.01401159n^3 - 0.53344205n^2 + 10.29494376n + 0.95414985, \\ B_L = 0.38, \\ B_L = 0.044833333n^3 - 1.1545n^2 + 9.81366667n - 27.095, \quad \text{if} \quad 7 \leqslant n \leqslant 10. \end{cases} \tag{37}$$

for monocycloparaffins,

$$\begin{cases} A_L = -3.60049 \times 10^{-3}n^3 + 0.04521772n^2 + 4.01286599n + 20.92204848, \\ B_L = 0.38, \\ B_L = 0.382, \quad \text{if} \quad n = 7. \end{cases} \tag{38}$$

for dicycloparaffins,

$$\begin{cases} A_L = -0.21151616n^3 + 7.44189329n^2 - 80.90626739n + 333.14012965, \\ B_L = 0.38. \end{cases} \tag{39}$$

for alkylbenzenes,

$$\begin{cases} A_L = -0.01015154n^3 + 0.56325414n^2 - 3.65181645n + 52.98586128, \\ B_L = -4.8006 \times 10^{-4}n^3 + 0.01880347n^2 - 0.2322112n + 1.2884813. \end{cases} \tag{40}$$

for cycloaromatics,

$$\begin{cases} A_L = -0.16622778n^3 + 6.12692857n^2 - 70.25798413n + 318.35692381, \\ B_L = 0.38, \\ B_L = -0.112n + 1.428, \quad \text{if} \quad n = 9, 10. \end{cases} \tag{41}$$

for alkylnaphthalenes,

$$\begin{cases} A_L = -0.04475185n^3 + 1.9486623n^2 - 23.16606442n + 152.2001, \\ B_L = -8.66667 \times 10^{-3}n^3 + 0.3145n^2 - 3.78483333n + 15.53, \\ B_L = 0.38, \quad \text{if} \quad n = 13, 15. \end{cases} \tag{42}$$

1.1.7. Saturated vapor pressure

Following [4] and using data provided in [1], the dependencies of saturated vapor pressure on carbon number and droplet surface temperature are approximated by the following equations:

$$p_{\text{sat}} = 10^{A_p - \frac{B_p}{T + C_p}} \times 133.322387415, \tag{43}$$

where T is in °C and the coefficients A_p, B_p and C_p for each hydrocarbon group are:

for n-paraffins,

$$\begin{cases} A_p = 1.729 \times 10^{-4}n^3 - 8.90265 \times 10^{-3}n^2 + 0.15972231n + 6.32493506, \\ B_p = 0.42901709n^3 - 19.62526141n^2 + 348.74864857n - 271.18350649, \\ C_p = 0.07338086n^3 - 2.8025752n^2 + 28.16525173n + 140.3191029. \end{cases} \tag{44}$$

for iso-paraffins,

$$\begin{cases} A_p = -4.6396 \times 10^{-4}n^3 + 0.01791282n^2 - 0.21598098n + 7.85098323, \\ A_p = -9.17 \times 10^{-3}n^2 + 0.16612n + 6.38501, \quad \text{if} \quad 8 \leqslant n \leqslant 10, \\ B_p = 0.40284641n^3 - 16.09970252n^2 + 251.44656196n + 262.57155844, \\ C_p = 0.05250932n^3 - 1.63418332n^2 + 6.50947219n + 251.7032977. \end{cases} \tag{45}$$

for monocycloparaffins,

$$\begin{cases} A_p = -2.0264 \times 10^{-4} n^3 + 0.01027486 n^2 - 0.17190187 n + 7.79361147, \\ B_p = 0.12405983 n^3 - 5.66221445 n^2 + 131.48430847 n + 746.06058275, \\ C_p = -0.05383683 n^3 + 2.32390793 n^2 - 35.83641142 n + 381.36450816. \end{cases} \quad (46)$$

for dicycloparaffins,

$$\begin{cases} A_p = 2.90646 \times 10^{-3} n^3 - 0.09640732 n^2 + 1.04406791 n + 3.28678719, \\ B_p = 2.00133838 n^3 - 72.24837662 n^2 + 921.33511183 n - 2355.50867965, \\ C_p = 0.2047096 n^3 - 7.0249632 n^2 + 74.00056962 n - 34.47946753. \end{cases} \quad (47)$$

for alkylbenzenes,

$$\begin{cases} A_p = 1.1956 \times 10^{-4} n^3 - 3.44724 \times 10^{-3} n^2 + 0.06802439 n + 6.76796999, \\ B_p = 0.08982906 n^3 - 6.15867299 n^2 + 193.77953324 n + 351.23931402, \\ C_p = 6.2217 \times 10^{-3} n^3 - 0.50178965 n^2 + 4.6466855 n + 219.98779276. \end{cases} \quad (48)$$

for cycloaromatics,

$$\begin{cases} A_p = -1.4837 \times 10^{-4} n^3 + 0.01522933 n^2 - 0.29303564 n + 8.70964201, \\ A_p = 7.07391, \quad \text{if} \quad n = 11, \\ B_p = 0.07888889 n^3 + 4.55285714 n^2 - 88.2229365 n + 2110.11381, \\ C_p = -0.0121 n^3 + 5.45827381 n^2 - 84.0731071 n + 625.767333. \end{cases} \quad (49)$$

for alkylnaphthalenes,

$$\begin{cases} A_p = 8.64034 \times 10^{-3} n^3 - 0.32482139 n^2 + 4.07331789 n - 9.71979122, \\ A_p = 7.10905, \quad \text{if} \quad n = 12, \\ B_p = 6.17222222 n^3 - 222.169762 n^2 + 2715.4823 n - 9235.68, \\ C_p = 0.57264815 n^3 - 20.4402698 n^2 + 236.464082 n - 677.375714. \end{cases} \quad (50)$$

1.2. Surrogates properties

The surrogates properties are calculated using the same expressions presented previously for Jet A and they come from the same database. However, as the coefficients used in the expressions are different, they are showed in the next sections for each property and each surrogate component.

1.2.1. Critical temperature

Comp	T_{cr}	p_{cr}
1	568.70	24.90
2	617.70	21.10
3	658.00	18.20
4	693.00	15.70
5	723.00	14.00
6	530.40	27.40
7	559.64	24.84
8	650.75	19.79
9	725.72	14.77
10	572.19	34.80
11	708.63	19.56
12	687.05	32.00
13	740.84	26.38
14	701.48	26.38
15	697.11	26.38
16	591.79	41.08
17	630.37	37.32
18	638.35	32.00
19	637.36	32.10
20	744.47	21.04
21	720.00	36.50

Table 3: Critical temperature and pressure for each surrogate component.

1.2.2. Liquid density

Comp	A_ρ	B_ρ	C_ρ
1	0.23220	0.26024	0.26940
2	0.23590	0.25668	0.28570
3	0.23440	0.25231	0.28960
4	0.23540	0.25561	0.27348
5	0.24350	0.25447	0.32380
6	0.23800	0.26963	0.27900
7	0.23410	0.26200	0.27130
8	0.24282	0.25391	0.28571
9	0.24467	0.26337	0.28571
10	0.26680	0.27028	0.29270
11	0.26180	0.26826	0.28571
12	0.28800	0.27116	0.29520
13	0.28597	0.26757	0.28571
14	0.28597	0.26369	0.28571
15	0.28597	0.26475	0.28571
16	0.29180	0.26188	0.29889
17	0.28760	0.26513	0.27410
18	0.27320	0.25222	0.29130
19	0.27760	0.25914	0.27982
20	0.27210	0.25690	0.32095
21	0.29980	0.25893	0.26770

Table 4: Coefficients to calculate liquid density for each surrogate component based on Eq. 3.

1.2.3. Liquid dynamic viscosity

Comp	A_μ	B_μ	C_μ	D_μ
1	-5.9245	888.09	1.2955×10^{-2}	-1.3596×10^{-5}
2	-6.0716	1017.70	1.2247×10^{-2}	-1.1892×10^{-5}
3	-7.0687	1253.00	1.3735×10^{-2}	-1.2215×10^{-5}
4	-7.8717	1446.70	1.4940×10^{-2}	-1.2495×10^{-5}
5	-8.1894	1557.10	1.5270×10^{-2}	-1.2371×10^{-5}
6	-7.2033	979.69	1.6986×10^{-2}	-1.7924×10^{-5}
7	-4.8603	715.64	1.0793×10^{-2}	-1.2293×10^{-5}
8	-4.6058	827.75	7.8684×10^{-3}	-7.3286×10^{-6}
9	-5.7519	1086.50	9.4927×10^{-3}	-7.7577×10^{-6}
10	-1.9879	508.06	1.2152×10^{-3}	-2.7318×10^{-6}
11	-7.9515	1529.10	1.4023×10^{-2}	-1.1002×10^{-5}
12	-3.6981	916.71	3.9609×10^{-3}	-2.9206×10^{-6}
13	-4.6518	910.91	7.5034×10^{-3}	-6.2957×10^{-6}
14	-4.5546	858.14	7.5743×10^{-3}	-6.6918×10^{-6}
15	-4.3915	836.22	7.1422×10^{-3}	-6.2706×10^{-6}
16	-5.6379	910.54	1.0861×10^{-2}	-1.0251×10^{-5}
17	-7.8805	1250.00	1.6116×10^{-2}	-1.3993×10^{-5}
18	-6.9452	1127.60	1.3933×10^{-2}	-1.2344×10^{-5}
19	-4.8328	832.75	8.9147×10^{-3}	-8.5136×10^{-6}
20	-9.0835	1599.90	1.7555×10^{-2}	-1.3886×10^{-5}
21	-6.3710	1274.00	1.0494×10^{-2}	-8.1163×10^{-6}

Table 5: Coefficients to calculate liquid dynamic viscosity for each surrogate component based on Eq. 11.

160 *1.2.4. Liquid thermal conductivity*

Comp	A_k	B_k	C_k
1	0.2229	-3.2988×10^{-4}	5.4691×10^{-8}
2	0.2218	-3.2560×10^{-4}	1.1282×10^{-7}
3	0.2292	-3.5926×10^{-4}	0
4	0.1956	-2.0000×10^{-4}	0
5	0.1996	-2.0000×10^{-4}	0
6	0.1864	-2.5000×10^{-4}	0
7	0.1900	-2.5667×10^{-4}	0
8	0.1938	-2.5000×10^{-4}	0
9	0.2018	-2.5000×10^{-4}	0
10	0.1555	-1.0944×10^{-4}	0
11	0.1793	-2.0000×10^{-4}	0
12	0.2076	-2.5000×10^{-4}	0
13	0.1550	-1.5556×10^{-4}	0
14	0.1550	-1.5556×10^{-4}	0
15	0.2091	-2.5000×10^{-4}	0
16	0.2099	-2.8557×10^{-4}	2.6919×10^{-8}
17	0.1873	-1.4690×10^{-4}	-1.2259×10^{-7}
18	0.1935	-2.4126×10^{-4}	5.9259×10^{-8}
19	0.1945	-2.0333×10^{-4}	0
20	0.1935	-2.0000×10^{-4}	0
21	0.1500	-6.6667×10^{-5}	0

Table 6: Coefficients to calculate liquid thermal conductivity for each surrogate component based on Eq. 19.

1.2.5. Specific heat capacity

Comp	A_c	B_c	C_c	D_c
1	82.736	1.3043	-3.8254×10^{-3}	4.6459×10^{-6}
2	79.741	1.6926	-4.5287×10^{-3}	4.9769×10^{-6}
3	84.485	2.0358	-5.0981×10^{-3}	5.2186×10^{-6}
4	111.814	2.2092	-5.2555×10^{-3}	5.0865×10^{-6}
5	89.101	2.7062	-6.1478×10^{-3}	5.7520×10^{-6}
6	115.052	0.6577	-2.1698×10^{-3}	3.3303×10^{-6}
7	134.965	0.8146	-2.5182×10^{-3}	3.5416×10^{-6}
8	213.729	1.0747	-2.8164×10^{-3}	3.4514×10^{-6}
9	258.868	1.5606	-3.8431×10^{-3}	4.1357×10^{-6}
10	103.668	0.4622	-1.3973×10^{-3}	2.0550×10^{-6}
11	211.195	0.9626	-2.3470×10^{-3}	2.7780×10^{-6}
12	108.262	0.9578	-2.3377×10^{-3}	2.4579×10^{-6}
13	190.982	0.4250	-9.2118×10^{-4}	1.1739×10^{-6}
14	180.486	0.4898	-1.1269×10^{-3}	1.4549×10^{-6}
15	185.965	0.4531	-1.0267×10^{-3}	1.3443×10^{-6}
16	83.703	0.5167	-1.4910×10^{-3}	1.9725×10^{-6}
17	56.460	0.9493	-2.4902×10^{-3}	2.6838×10^{-6}
18	123.471	0.6197	-1.6883×10^{-3}	2.1608×10^{-6}
19	83.637	0.8786	-2.3192×10^{-3}	2.5989×10^{-6}
20	139.356	0.7940	-1.8805×10^{-3}	2.3121×10^{-6}
21	154.318	0.3523	-7.7637×10^{-4}	1.0223×10^{-6}

Table 7: Coefficients to calculate liquid specific heat capacity for each surrogate component based on Eq. 27.

1.2.6. Latent heat of evaporation

Comp	A_L	B_L
1	59.0771	0.439
2	71.4282	0.451
3	77.1658	0.407
4	86.8851	0.418
5	96.6800	0.422
6	49.9169	0.408
7	59.5032	0.481
8	70.7797	0.380
9	87.1109	0.380
10	49.4195	0.415
11	73.9481	0.380
12	58.8676	0.380
13	67.8685	0.380
14	64.0928	0.380
15	65.0708	0.380
16	50.1390	0.383
17	55.6060	0.375
18	60.1072	0.397
19	60.0700	0.365
20	81.3400	0.410
21	59.4549	0.308

Table 8: Coefficients to calculate latent heat of evaporation for each surrogate component based on Eq. 35.

1.2.7. Saturated vapor pressure

Comp	A_p	B_p	C_p
1	7.14462	1498.96	225.874
2	7.21745	1693.93	216.459
3	7.22883	1807.47	199.381
4	7.26165	1914.86	183.519
5	7.36235	2094.08	180.407
6	7.05830	1340.21	230.768
7	7.12709	1473.84	229.440
8	7.03727	1632.18	181.835
9	7.07426	1828.55	154.450
10	7.00107	1375.13	232.819
11	7.10051	1835.18	189.998
12	6.82768	1544.81	204.090
13	6.90824	1729.18	194.350
14	6.91430	1643.57	199.480
15	6.91266	1665.76	198.150
16	7.13620	1457.29	231.827
17	7.14914	1566.59	222.596
18	7.18167	1655.21	225.615
19	7.26105	1695.83	222.415
20	7.25666	1945.86	198.582
21	7.16735	1806.14	213.732

Table 9: Coefficients to calculate saturated vapor pressure for each surrogate component based on Eq. 43.

References

[1] C. Yaws, Yaws' Handbook of Thermodynamic and Physical Properties of Chemical Compounds, Knovel, 2003.

[2] C. Yaws, (Eds.), Thermophysical properties of chemicals and hydrocarbons, William Andrew, Norwich, NY, 2008.

[3] C. Yaws, (Eds.), Transport properties of chemicals and hydrocarbons: viscosity, thermal conductivity, and diffusivity of C1 to C100 organics and Ac to Zr inorganic, William Andrew, 2009.

[4] S. S. Sazhin, M. Al Qubeissi, R. Nasiri, V. M. Gun'ko, A. E. Elwardany, F. Lemoine, F. Grisch, M. R. Heikal, A multi-dimensional quasi-discrete model for the analysis of diesel fuel droplet heating and evaporation, Fuel 129 (2014) 238 – 266. doi:10.1016/j.fuel.2014.03.028.